

Inhibition of low molecular weight protein tyrosine phosphatase by an induced-fit mechanism

Rongjun He, Jifeng Wang, Zhi-Hong Yu, Ruo-Yu Zhang, Sijiu Liu, Li Wu, and Zhong-Yin Zhang

J. Med. Chem., **Just Accepted Manuscript** • Publication Date (Web): 27 Sep 2016

Downloaded from <http://pubs.acs.org> on September 28, 2016

Just Accepted

“Just Accepted” manuscripts have been peer-reviewed and accepted for publication. They are posted online prior to technical editing, formatting for publication and author proofing. The American Chemical Society provides “Just Accepted” as a free service to the research community to expedite the dissemination of scientific material as soon as possible after acceptance. “Just Accepted” manuscripts appear in full in PDF format accompanied by an HTML abstract. “Just Accepted” manuscripts have been fully peer reviewed, but should not be considered the official version of record. They are accessible to all readers and citable by the Digital Object Identifier (DOI®). “Just Accepted” is an optional service offered to authors. Therefore, the “Just Accepted” Web site may not include all articles that will be published in the journal. After a manuscript is technically edited and formatted, it will be removed from the “Just Accepted” Web site and published as an ASAP article. Note that technical editing may introduce minor changes to the manuscript text and/or graphics which could affect content, and all legal disclaimers and ethical guidelines that apply to the journal pertain. ACS cannot be held responsible for errors or consequences arising from the use of information contained in these “Just Accepted” manuscripts.

1
2
3
4
5
6
7 **Inhibition of low molecular weight protein tyrosine phosphatase by an induced-fit**
8
9 **mechanism**
10

11
12
13
14
15 Rongjun He[#], Jifeng Wang[#], Zhi-Hong Yu, Ruo-Yu Zhang, Sijiu Liu, Li Wu, Zhong-Yin Zhang^{*}
16
17

18
19
20 Department of Medicinal Chemistry and Molecular Pharmacology, Department of Chemistry, Center for
21
22 Cancer Research, and Institute for Drug Discovery, Purdue University, 720 Clinic Drive, West
23
24 Lafayette, IN 47907
25
26
27
28
29
30
31
32

33
34 Running Title: Highly Selective Inhibitors of LMW-PTP
35
36
37
38
39
40
41
42
43
44
45
46
47
48
49
50
51
52
53
54
55
56
57
58
59
60

Abstract

The low molecular weight protein tyrosine phosphatase (LMW-PTP) is a regulator of a number of signaling pathways and has been implicated as a potential target for oncology and diabetes/obesity. There is significant therapeutic interest in developing potent and selective inhibitors to control LMW-PTP activity. We report the discovery of a novel class of LMW-PTP inhibitors derived from SulfoPhenyl Acetic Amide (SPAA), some of which exhibit greater than 50-fold preference for LMW-PTP over a large panel of PTPs. X-ray crystallography reveals that binding of SPAA-based inhibitors induces a striking conformational change in the LMW-PTP active site, leading to the formation of a previously undisclosed hydrophobic pocket to accommodate the α -phenyl ring in the ligand. This induced-fit mechanism is likely a major contributor responsible for the exquisite inhibitor selectivity.

Introduction

As a major posttranslational modification mechanism, protein tyrosine phosphorylation regulates numerous cellular processes including growth, differentiation, migration, and survival.¹ Proper level of protein tyrosine phosphorylation, which is dynamically maintained by protein tyrosine kinases (PTKs) and protein tyrosine phosphatases (PTPs), is essential for normal cellular homeostasis. Perturbation to the balance between PTK and PTP activity induces either excessive or diminished substrate phosphorylation, which is associated with a wide range of pathological conditions such as cancer, diabetes and autoimmune disorders.^{1,2} Consequently, the ability to selectively modulate signaling pathways mediated by protein tyrosine phosphorylation holds enormous potential for therapeutic intervention, as evidenced by the development of PTK inhibitors for various clinical indications.³ Given the substantial success of PTK inhibitors, there is heightened interest in targeting the opposing PTPs for therapeutic applications.

The PTPs constitute a large family of signaling enzymes (>100) that can be broadly classified into three groups: tyrosine-specific, dual-specific, and the low molecular weight protein tyrosine phosphatase (LMW-PTP).⁴ The common feature of all PTPs is the active site sequence C(X)₅R(S/T), also known as the PTP signature motif or P-loop, which specifically binds the phosphoryl moiety of the substrate. As an enigmatic member of the PTP family, the LMW-PTP, encoded by *Acp1*, is an 18 kDa cytosolic enzyme found ubiquitously in both prokaryotic and eukaryotic organisms.⁵⁻⁸ LMW-PTP has been shown to either positively or negatively regulate the function of platelet-derived growth factor receptor (PDGFR),⁹⁻¹¹ fibroblast growth factor receptor (FGFR),¹² epidermal growth factor receptor (EGFR),¹³ insulin receptor (IR),^{10,14,15} and is involved in numerous signaling cascades including focal adhesion kinase (FAK),^{16,17} STAT5,^{18,19} and Epherin.^{20,21} However, the mechanism(s) by which these pathways are controlled by LMW-PTP is not yet fully understood.

1
2
3 A number of studies suggest LMW-PTP as a potential oncoprotein. Increased expression of
4 LMW-PTP mRNA and protein levels were observed in malignant samples of breast, colon, bladder and
5
6
7
8 kidney.^{22,23} More recently, LMW-PTP was reported to enhance the metastatic potential of prostate
9
10 cancer cells, resulting in worse patient survival.²⁴ LMWPTP is also overexpressed and active in primary
11
12 colorectal cancer.²⁵ Interestingly, LMW-PTP has also been implicated in the development of type II
13
14 diabetes and obesity.²⁶⁻²⁸ For example, LMW-PTP was implicated as a negative regulator of insulin
15
16 signaling through dephosphorylation of components in the IR pathway.^{10,14} Diet-induced obese mice
17
18 treated with LMW-PTP antisense oligonucleotide exhibited decreased plasma insulin, glucose,
19
20 triglyceride and cholesterol levels, and showed increased glucose and insulin tolerance.¹⁵
21
22
23
24

25 In view of the emerging recognition of LMW-PTP as a potential target for oncology and
26
27 diabetes/obesity, there is considerable interest in obtaining small molecule inhibitors of LMW-PTP as
28
29 potential therapeutics.^{8,29-37} Moreover, potent and selective inhibitors of LMW-PTP would be invaluable
30
31 tools for interrogating LMW-PTP biology and therapeutic hypothesis testing. Unfortunately, reported
32
33 inhibitors lack robust selectivity for LMW-PTP and therefor are not suitable as chemical probes for
34
35 further mechanistic studies and ultimately, for the development of therapeutic agents targeting LMW-
36
37 PTP. We describe the identification and characterization of a novel series of LMW-PTP inhibitors,
38
39 which exhibit greater than 50-fold preference for LMW-PTP over a large panel of PTPs. Crystal
40
41 structures of LMW-PTP-inhibitor complexes reveal a ligand induced conformational change in LMW-
42
43 PTP that is responsible for the exquisite inhibitor selectivity.
44
45
46
47
48
49
50
51

52 Results and Discussion

53
54 *Acquisition of potent and selective LMW-PTP inhibitors.* The PTPs, as a target class, have
55
56 presented significant difficulties for drug discovery. The high sequence and structure homology within
57
58
59
60

1
2
3 the PTP active site creates a challenge in achieving inhibitor selectivity among closely related family
4 members. In addition, the positive-charged environment of the PTP active site poses unique drug
5 discovery challenges, as most competitive inhibitors by necessity are negatively charged, which
6 complicates drug development due to low cell permeability and bioavailability. Since existing drugs are
7 already endowed with favorable pharmacokinetic properties, we sought to harness the privileged drug
8 space for novel PTP inhibitory scaffolds that can be further optimized into potent and selective PTP
9 inhibitors with improved drug-like properties. To this end, we have recently discovered SulfoPhenyl
10 Acetic Amide (SPAA), a fragment originated from cefsulodin, as a novel pTyr mimetic.³⁸ We found that
11 SPAA inhibited LMW-PTP with an IC_{50} of 2 mM, as opposed to an IC_{50} of >50 mM for PTP1B and
12 SHP2. LMW-PTP exists in two isoforms (namely LMW-PTPA and LMW-PTPB, respectively) which
13 differ only by a loop that flanks the catalytic site. This study concerns mostly the LMW-PTPA isoform.
14 In order to increase the potency and selectivity of SPAA for LMW-PTP, we sought to capture additional
15 interactions outside of the active site pocket. To this end, we prepared a SPAA-based focused library by
16 reacting α -sulfophenyl acetic acid with a set of 192 amines of different size, charge, and lipophilicity.³⁸
17 The library was assembled directly on 96-well plates under standard HBTU amide coupling conditions.
18 Reactions from representative wells were monitored by LC-MS, which indicated a 70-80% product
19 conversion.

20
21
22
23
24
25
26
27
28
29
30
31
32
33
34
35
36
37
38
39
40
41
42
43
44
45
46
47
48
49
50
51
52
53
54
55
56
57
58
59
60
Library compounds were screened for inhibitory activity against LMW-PTP at a compound concentration of ~ 10 μ M, and counter-screened against PTP1B and SHP2 to provide preliminary specificity information. Several compounds, **1**, **2**, **3**, **4**, **5**, **6**, **7**, **8** (Figure 1), exhibited >50% inhibition against LMW-PTP, but <10% inhibition against PTP1B and SHP2, indicating significant specificity for LMW-PTP. These hits were resynthesized and purified with reversed-phase HPLC, and their IC_{50} values against LMW-PTP were measured, which are summarized in Figure 1. To our delight, all of the hits

1
2
3 display IC_{50} values less than 10 μM , consistent with our initial screening results. This represents a more
4
5 than 200-fold gain in binding affinity compared to the parent SPAA. Kinetics studies with compound **7**
6
7 were carried out to probe its mode of inhibition. Figure 2 showed that **7** is a competitive inhibitor against
8
9 LMW-PTPA with a K_i of $3.2 \pm 0.1 \mu\text{M}$. We also determined that compound **7** inhibits the LMW-PTPB
10
11 isoform with a K_i of $1.7 \pm 0.1 \mu\text{M}$, indicating that the SPAA-based inhibitors likely inhibit both LMW-
12
13 PTP isoforms with similar potency. Structure and activity survey revealed that the aniline containing
14
15 compound **9** and the 2-aminothiazole containing compound **10** have significantly reduced activities,
16
17 indicating that substituents on aniline (compound **9** vs compounds **1**, **2**, **3**, **4**, **5**, **8**) and the second
18
19 benzene ring (compound **10** vs compound **7**) are required for high affinity binding. The propyl amine
20
21 containing compound **11** is inactive as expected given that it does not have an aromatic group at the
22
23 amine terminal, and it was inactive in our initial screening. To gain a more comprehensive picture of
24
25 how selective these compounds are to the LMW-PTP, we broadened the scope of selectivity profiling by
26
27 inclusion of an additional 22 phosphatases in addition to PTP1B and SHP2. As shown in Table 1,
28
29 compounds **3**, **5**, and **6** exhibit no inhibitory activity against any of the phosphatases in the panel at 200
30
31 μM concentration. In particular, compound **3** possesses a greater than 35-fold preference for LMW-PTP
32
33 over all other PTPs.
34
35
36
37
38
39
40
41

42 *Structural basis of LMW-PTP inhibition by the SPAA-based inhibitors.* To elucidate the
43
44 structural basis of LMW-PTP inhibition and to aid the design of more potent and selective LMW-PTP
45
46 inhibitors, we sought to determine the crystal structures of LMW-PTP in complex with the SPAA-based
47
48 inhibitors. We initially obtained LMW-PTP crystals under previously published conditions including
49
50 100 mM MES buffer, 30% PEGME 5,000 and 0.2 M ammonium sulfate³⁹ in the presence of 1 mM
51
52 compound **7**. The structure was determined by molecular replacement, using the published LMW-PTP
53
54 structure as the search model (PDBID:5PNT). However, compound **7** was nowhere to be found. Instead,
55
56
57
58
59
60

1
2
3 a MES molecule occupied the active site (Figure 3A). MES is a weak inhibitor of LMW-PTP, with an
4
5 IC_{50} greater than 10 mM. The sulfonic acid moiety mimics the interaction of the PO_4 group of a
6
7 substrate within the phosphatase active site. The rest of the molecule interacts with the surrounding
8
9 residues by van der Waals interactions. We then systematically screened alternate crystallization
10
11 conditions without MES and finalized 25-30% PEGME 5,000 in 100 mM Bis-Tris, pH 6.0-6.5 for
12
13 optimal crystal growth of the LMW-PTP•7 complexes. Again, the structure of LMW-PTP•7 was
14
15 determined by molecular replacement, and compound 7 was unambiguously identified around the
16
17 C(X)₅R(S/T) PTP signature motif (Figure 3B). For comparison, we also crystallized and solved the
18
19 structure of LMW-PTP in complex with compound 9, which has an $IC_{50} > 100 \mu M$, under the same
20
21 conditions (Figure 3C). Finally, by soaking the LMW-PTP•MES crystals in 100 mM Bis-Tris buffer, we
22
23 obtained the crystal structure of apo LMW-PTP (Figure 3D). In the apo LMW-PTP structure, the MES
24
25 molecule is replaced by three water molecules, which are well organized to form hydrogen bonds with
26
27 the amides of the P-loop residues. The data collection and refinement statistics for all four crystal
28
29 structures are summarized in Table 2. The overall LMW-PTP structures are very similar and the root
30
31 mean square derivation (rmsd) for all $C\alpha$ atoms is 0.341 Å between LMW-PTP•7 and LMW-PTP•MES,
32
33 0.529 Å between LMW-PTP•7 and LMW-PTP•9, and 0.630 between LMW-PTP•7 and the apo
34
35 enzyme.
36
37
38
39
40
41
42
43
44

45 Although the overall three-dimensional structures are quite similar between LMW-PTP•7 and
46
47 LMW-PTP•MES, superimposition of both structures revealed a localized conformational change in the
48
49 active site. In the LMW-PTP•MES complex, the side chain dihedral angle χ_1 ($\angle C-CA-CB-SG$) of
50
51 Cys17, which is located in the P-loop, is 167.2 degree, while in the presence of compound 7, the side
52
53 chain of Cys17 is pushed 114.3 degree away by the α -phenyl ring in 7, adapting a new χ_1 of 52.9 degree
54
55 (Figure 4A). In addition, the movement of the Cys17 side chain also shifts the P-loop downward by 1.4
56
57
58
59
60

1
2
3 Å from its original position (Figure 4A). Interestingly, the conformation of the side chain of Cys17 in
4
5 the apo form of LMW-PTP is identical to that observed in LMW-PTP•MES structure (Figure 4B), while
6
7 the side chain of Cys17 exists in the same conformation in both LMW-PTP•9 and LMW-PTP•7
8
9 structures (Figure 4C). The net result of this SPAA ligand induced conformational change is the creation
10
11 of a hydrophobic cavity constituted by residues Ile16, Cys17, Pro130, Tyr131, Phe138 and the side-
12
13 chain aliphatic atoms of Asp56, which is well suited for the α -phenyl ring in compound 7 and 9 (Figure
14
15 4D). To the best of our knowledge, no other PTPs undergo this structural change in the active site upon
16
17 ligand binding.
18
19
20
21
22

23 To better understand the unique preference of SPAA for LMW-PTP, we compared the active site
24
25 features of LMW-PTP with those of PTP1B, a representative of the classical PTPs. As shown in Figure
26
27 5A, sequence alignment and structure superimposition of the signature motif $C(X)_5R(S/T)$ of LMW-
28
29 PTP•7 with that of the PTP1B structure (PDBID: 1PXH) revealed that: 1) although the backbones of the
30
31 two signature motifs align very well but only 3 of 7 residues are conserved between LMW-PTP and
32
33 PTP1B, making the active site pockets rather different in shape and electrostatic potential between the
34
35 two enzymes; 2) Cys17 plays a key role in the induce-fit process to create a hydrophobic cavity
36
37 accommodating the α -phenyl ring of compound 7, but the corresponding residue in PTP1B (and other
38
39 classical PTPs) is Gly220, which is incapable of doing the same; 3) a severe steric clash exists between
40
41 the α -phenyl ring and Gln262, and another between the benzothiazole and Tyr46. Since the conserved
42
43 Gln262 and Tyr46 come from the adjacent active site Q-loop and pY-loop of PTP1B, steric clashes may
44
45 exist whether the WPD-loop is in the closed (Figure 5B) or open conformation (Figure 5C).
46
47 Collectively, the active site specificity manifested by the induced-fit mechanism is unique for LMW-
48
49 PTP, and likely responsible, in large part, for SPAA's preference to the LMW-PTP over PTP1B, SHP2
50
51 and other PTPs as well.
52
53
54
55
56
57
58
59
60

1
2
3 In addition to revealing a novel induced-fit mechanism for LMW-PTP inhibition by the SPAA-
4
5 containing inhibitors, the structure of LMW-PTP•**7** also uncovers the basis for its potency: the sulfonic
6
7 acid moiety is in close proximity to the P-loop and is stabilized by six hydrogen bonds with main chain
8
9 amides of Leu13, Gly14, Ile16, Cys17, Arg18 and the side chain amide of Arg18 (Figure 6) with a
10
11 distance ranging from 2.8 to 3.2 Å. In addition, the amide NH of compound **7** forms a hydrogen bond
12
13 with carboxylate O of the general acid Asp129 with a distance of 3.0 Å. This is a new interaction that
14
15 was never observed in previously reported LMW-PTP inhibitors. Moreover, a water molecule bridges
16
17 another two hydrogen bonds between the N atom within thiazole and the carboxylate O of Asp129.
18
19 Besides the hydrogen bond interactions mentioned above, compound **7** is also involved in a network of
20
21 π - π interactions with LMW-PTP (Figure 6). π - π interaction has long been acknowledged as an integral
22
23 force in maintaining protein stability^{40,41} as well as in differential recognition of medicinal agents
24
25 containing aromatic substituents by their protein targets.⁴² In the unliganded state, the phenyl ring of
26
27 Tyr131 is parallel to that of Tyr49 on the opposite side of the empty active site, with a distance of ~9.9
28
29 Å between the two aromatic rings. When compound **7** is bound in the active site, the benzothiazole ring
30
31 of **7** is sandwiched between the phenyl rings of Tyr49 and Tyr131. The distance of the closest atoms
32
33 between the phenyl ring of Tyr49 and the benzothiazole ring is ~3.5 Å. Similarly, the distance of the
34
35 closest atoms between the phenyl ring of Tyr131 and the benzothiazole ring is ~3.8 Å. Hence, the
36
37 benzothiazole ring falls within the London dispersion distance with both of these tyrosine residues.⁴³
38
39 The position and orientation of the Tyr131 side chain is constrained by Tyr132 through an edge to face
40
41 π - π interaction, with the distance of ~4.0 Å (mass center to mass center) (Figure 6). Tyr131 not only
42
43 forms a π - π interaction with the phenyl ring of benzothiazole moiety, it also forms an edge to face π - π
44
45 interaction with the α -phenyl ring of **7**, with a distance of ~4.2 Å (Figure 6). Taken together, these π - π
46
47 interactions form a network involving three tyrosine residues from LMW-PTP (Tyr49, Tyr131 and
48
49
50
51
52
53
54
55
56
57
58
59
60

1
2
3 Tyr132) and the benzothiazole and α -phenyl ring from compound **7**. These interactions, in addition to
4
5 those mentioned above, likely play a major role for tight binding of compound **7**.
6
7

8
9 In order to understand why installation of a double aromatic ring to the SPAA moiety generated
10 much better inhibitors for LMW-PTP than did the single ring counterparts (Figure 1), we also
11 determined the structure of LMW-PTP•**9**. Superimposition of the LMW-PTP•**9** structure to that of
12 LMW-PTP•**7** revealed that the sulfonic acid moiety and the α -phenyl ring of compound **9** are located at
13 exactly the same positions in the active site as the corresponding groups in compound **7** (Figure 4C).
14
15 However, the aniline ring of compound **9** overlaps with only half of the double aromatic benzothiazole
16 ring of compound **7**. Although it still forms a π - π interaction with Tyr131, the distance between the
17 aniline ring and Tyr49 increases to about 4.5 Å, significantly longer than what is required for optimal
18 London dispersion interaction. Moreover, the nonpolar benzene ring also eliminates the water-bridged
19 hydrogen bonds interaction with Asp129. Thus, the reduction in π - π interactions and water-bridged polar
20 interactions between LMW-PTP and the single benzene ring at the acetamide position may account for
21 the >15-fold decrease in inhibitory activity for compound **9** versus compound **7**. Compared to compound
22 **7**, the thiazole group in **10** may still retain the water-bridged hydrogen bond interactions but likely loses
23 the π - π interactions due to the absence of the terminal benzene ring. This may explain why compound
24 **10** is superior to compound **9** even though it has a smaller single aromatic ring, suggesting that
25 appropriately positioned polar atoms in the first aromatic ring will benefit binding affinity.
26
27
28
29
30
31
32
33
34
35
36
37
38
39
40
41
42
43
44
45
46

47 *Initial optimization of compound 7.* Based on the structural insights, we carried out an initial
48 structure-activity relationship study in order to lay the foundation to develop more potent and selective
49 LMW-PTP inhibitors. From the crystal structures, the α -phenyl ring is situated in a hydrophobic cavity,
50 bordered by residues Ile16, Cys17, Pro130, Tyr131, Phe138 and the side-chain aliphatic atoms of
51 Asp56. We explored whether installation of a small substituent on the α -benzene ring could capture
52
53
54
55
56
57
58
59
60

1
2
3 additional interactions with the enzyme, leading to increased binding affinity (Figure 7). Substituents to
4 enhance hydrophobic interactions included *ortho*-chloro (compound **13**), *ortho*-methyl (compound **14**),
5
6
7
8 *meta*-methyl (compound **16**), *para*-methyl (compound **20**), and *para*-bromo (compound **21**); and
9
10 substituents aimed for gaining potential hydrogen-bonding interactions included *ortho*-fluoro
11
12 (compound **12**), *meta*-fluoro (compound **15**), *meta*-nitrile (compound **17**), *meta*-nitro (compound **18**),
13
14 and *meta*-trifluoromethyl (compound **19**). We also introduced electron donating substituents (compound
15
16
17 **14**, **16**, **20**) and electron withdrawing substituents (compounds **17**, **18**, **19**) to ascertain whether
18
19 perturbation of electronic properties would influence potential π - π interactions and thereby inhibitor
20
21 activity. Unfortunately, we found that modifications to the α -phenyl ring led to significant diminished
22
23 inhibitory activity toward LMW-PTP, indicating that the ligand binding induced hydrophobic pocket
24
25 can only accommodate a naked benzene ring.
26
27
28
29

30 We next explored substituents on the benzothiazole ring in compound **7**. Analysis of the LMW-
31
32 PTP•**7** crystal structure showed that the amide NH of **7** forms a hydrogen bond with Asp129, and the
33
34 benzothiazole moiety forms strong π - π stacking interactions with Tyr49, Tyr131, and Tyr132. We
35
36 reasoned that by installing small substituents with appropriate electronic properties and polarities at the
37
38 benzene ring of benzothiazole, we could enhance the hydrogen bonding interaction between the amide
39
40 NH and Asp129, and/or hydrophobic and polar interactions between the benzothiazole moiety and Tyr
41
42 49, Tyr131, and Tyr132. Hence we designed and synthesized a series of compounds with electron
43
44 donating groups (compounds **23**, **24**, **25**, **29**, **31**), electron withdrawing groups (compounds **26**, **28**, **32**),
45
46
47 hydrophobic groups (**22**, **23**, **25**, **27**, **29**), and polar groups (compounds **24**, **26**, **28**, **30**, **31**, **32**). As
48
49 summarized in Figure 8, most derivatives displayed slightly increased activity over parent compound **7**.
50
51 Specifically, compound **28** with a nitro group at the 6 position and compound **32** with carboxylate group
52
53 at the 6 position are 3.5- and 2.5-fold more active than **7**, with a measured IC_{50} at $2.1 \pm 0.2 \mu\text{M}$ and $3.1 \pm$
54
55
56
57
58
59
60

1
2
3 0.1 μM , respectively. Nitro and carboxylate groups are both electron withdrawing which make the NH
4
5 amide bond more acidic, which likely enhances its hydrogen bonding interaction with Asp129. In
6
7 addition, the nitro and carboxylate groups are in close proximity to Tyr49, to make a new hydrogen-
8
9 bonding interaction with the hydroxyl group of Tyr49. Kinetics studies revealed that compound **28** is
10
11 also a competitive inhibitor for LMW-PTP with a K_i at $1.0 \pm 0.1 \mu\text{M}$. More importantly, compound **28**
12
13 exhibited at least over 50-fold selectivity for LMW-PTP over the panel of 24 phosphatases (Table 1),
14
15 making compound **28** the most potent and selective LMW-PTP inhibitor reported to date. Deletion of
16
17 the sulfonic acid in **28** completely abolishes compound **33**'s ability to inhibit LMW-PTP, consistent with
18
19 the importance of sulfonic acid for inhibition.
20
21
22
23
24

25 *Cellular activity of compound 28.* To assess the effects of **28** in insulin signaling pathway, we
26
27 pretreated HepG2 cells with **28** for 2 h and then stimulated the cells with 50 nM insulin for 30 min. As
28
29 shown in Figure 9A, compound **28** enhanced AKT phosphorylation in a dose-dependent manner relative
30
31 to the vehicle DMSO. To ensure that the cellular activity of compound **28** is due to inhibition of LMW-
32
33 PTP and not nonspecific effects, a structurally related but inactive analog of compound **28**, compound
34
35 **33** ($\text{IC}_{50} \gg 100 \mu\text{M}$ for LMW-PTP, Figure 8), was also evaluated. As expected, at 16 μM compound **33**
36
37 exerted no effect on insulin induced AKT phosphorylation while at the same concentration compound
38
39 **28** increased AKT phosphorylation by 260% (Figure 9B). The results indicate that compound **28**
40
41 promotes insulin induced AKT phosphorylation through specifically inhibiting LMW-PTP activity.
42
43
44
45
46

47 In summary, we have developed a novel class of LMW-PTP inhibitors based on SPAA by using
48
49 a focused library synthesis approach. High throughput screening and kinetic studies of the library
50
51 components led to the identification of a number of hits with excellent potency and selectivity for
52
53 LMW-PTP. Subsequent crystallography studies disclosed that sulfonic acid is in close proximity with
54
55 the active site PTP signature motif and stabilized by multiple hydrogen bonds. The structure also
56
57
58
59
60

1
2
3 revealed a striking ligand-induced conformational change in LMW-PTP that is essential for inhibitor
4 specificity. Moreover, the structure also identified a triad of aromatic residues Tyr49, Tyr131, and
5 Tyr132 that contribute to the potency and specificity of the inhibitors by forming strong π - π stacking
6 interactions with the aromatic moieties in the ligand. Structure-guided optimization of compound 7
7 resulted in compound **28**, which displayed a K_i value of $1.0 \pm 0.1 \mu\text{M}$ for LMW-PTP and an
8 unprecedented >50 fold selectivity for LMW-PTP over 24 other PTPs, marking it the first truly specific
9 LMW-PTP inhibitor. Our study provides a solid foundation upon which more potent and selective
10 LMW-PTP inhibitors can be designed. These compounds are also expected to serve as useful tools to
11 study LMW-PTP's biological function, and are excellent starting points for developing novel
12 therapeutics for cancer and type 2 diabetes.
13
14
15
16
17
18
19
20
21
22
23
24
25
26
27
28
29

30 Experimental Section

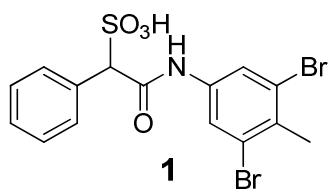
31
32
33 *Materials and General Procedures.* p-Nitrophenyl phosphate (pNPP) was purchased from Fluke.
34 Crystallization reagents were from Hampton Research. DNA primers were from Genwiz Inc. and other
35 reagents were obtained from Fisher or Sigma. Reagents were used as purchased from Sigma-Aldrich and
36 Fisher Scientific. ^1H and ^{13}C NMR spectra were obtained on a BrukerAvance II 500 MHz NMR
37 spectrometer with TMS or residual solvent as standard. Mass spectra were obtained using an Agilent
38 Technologies 6130 quadrupole LC/MS. HPLC purification was carried out on a Waters Delta 600
39 equipped with a Sunfire Prep C18 OBD column (30 mm/150 mm, 5 μm) with methanol water (both
40 containing 0.1% TFA) as mobile phase (gradient: 50-100% methanol, flow 10 mL/min). The purity of
41 all final tested compounds was established to be >95% by Agilent Technologies 6130 quadrupole
42 LC/MS by using methanol water (both containing 0.1% TFA) as the mobile phase (gradient: 0-100%
43 methanol, flow 1.0 mL/min), with UV monitoring at the fixed wavelength of 254 nm.
44
45
46
47
48
49
50
51
52
53
54
55
56
57
58
59
60

1
2
3
4
5
6
7
8
9
10
11
12
13
14
15
16
17
18
19
20
21
22
23
24
25
26
27
28
29
30
31
32
33
34
35
36
37
38
39
40
41
42
43
44
45
46
47
48
49
50
51
52
53
54
55
56
57
58
59
60

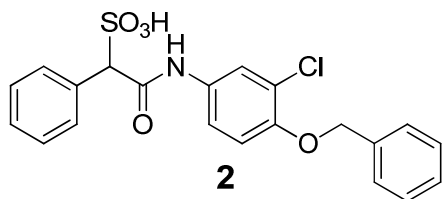
Library Synthesis. To all wells of 96-well plates were added sulfophenylacetic acid (20 μ L, 20 mM in DMF), HBTU (20 μ L, 20 mM in DMF), HOBt (20 μ L, 20 mM in DMF), DIEA (20 μ L, 60 mM in DMF), and corresponding 192 amines (He et al., 2015) from storage plates (1.2 μ L, 0.5 mM in DMF), the reaction plates were placed at rt for 1 day. The reaction wells from aniline were monitored by LC-MS to show that reactions occurred well in great conversions. Thus a library of 192 compounds was obtained with estimated concentration at 4 mM (assuming 80% product yield), which was screened against LMW-PTP and other PTPs. All compounds were prepared as racemic mixtures.

Representative Procedure for the Synthesis of Products. To α -Sulfophenyl acetyl chloride (0.234 g, 1 mmol) and DIEA (0.522 mL, 3 mmol) in DMF (2 mL) was added propyl amine (0.09 mL, 1.1mmol), the mixture was stirred at rt for 1 h. After quenching with water, it was subjected to HPLC purification, and product **11** was obtained as colorless oil (93% yield, >95% purity).

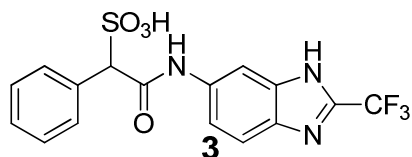
Characterizations of Compounds 1 to 33.



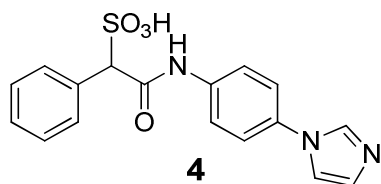
1: ^1H NMR (500 MHz, DMSO) δ 10.44 (s, 1H), 7.89 (s, 2H), 7.59-7.58 (m, 2H), 7.28-7.26 (m, 3H), 4.78 (s, 1H), 2.43 (s, 3H); ^{13}C NMR (500 MHz, DMSO) δ 166.5, 139.0, 134.8, 130.6, 130.0, 127.4, 127.0, 124.2, 121.8, 71.6, 22.6. ESI-HRMS Calcd. for $\text{C}_{15}\text{H}_{12}\text{Br}_2\text{NO}_4\text{S}$ ($\text{M}-\text{H}^+$): 459.8859; found 459.8866.



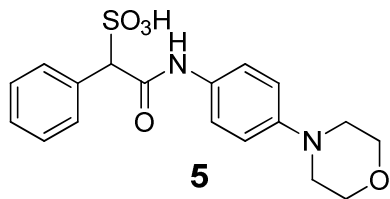
1
2
3 2: ^1H NMR (500 MHz, DMSO) δ 10.29 (s, 1H), 7.83 (d, $J = 1.7$ Hz, 1H), 7.57-7.56 (m, 2H), 7.46-7.17
4 (m, 10H), 5.15 (s, 2H), 4.73 (s, 1 H); ^{13}C NMR (DMSO) δ 165.9, 149.4, 136.7, 135.1, 133.2, 129.9,
5
6 128.5, 127.9, 127.5, 127.4, 126.9, 121.3, 120.5, 118.7, 114.7, 71.7, 70.3. ESI-HRMS Cacl.d.for
7
8 $\text{C}_{21}\text{H}_{17}\text{ClNO}_5\text{S}$ ($\text{M}-\text{H}^+$): 430.0521, found 430.0519.
9
10



23 3: ^1H NMR (500 MHz, DMSO) δ 10.48 (s, 1H), 8.23 (s, 1H), 7.67 (d, $J = 8.7$ Hz, 1H), 7.61 (d, $J = 7.3$
24 Hz, 2H), 7.35-7.25 (m, 4H), 4.82 (s, 1H); ^{13}C NMR (DMSO) δ 166.1, 139.92, 139.6, 136.4, 136.2,
25 135.5, 135.2, 129.9, 127.4, 127.0, 120.1, 118.2, 118.0, 116.9, 104.1, 71.8. ESI-HRMS Cacl.d.for
26 $\text{C}_{16}\text{H}_{11}\text{F}_3\text{N}_3\text{O}_4\text{S}$ ($\text{M}-\text{H}^+$): 398.0428; found 398.0434.
27
28
29
30
31
32
33
34
35



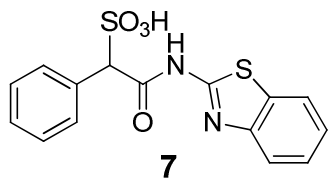
44 4: ^1H NMR (500 MHz, DMSO) δ 10.60 (s, 1H), 9.65 (t, $J = 1.3$ Hz, 1H), 8.26 (t, $J = 1.7$ Hz, 1H), 7.90 (t,
45 $J = 1.6$ Hz, 1H), 7.84-7.83 (m, 2H), 7.76-7.73 (m, 2H), 7.59-7.58 (m, 2H), 7.30-7.24 (m, 3H), 4.80 (s,
46 1H); ^{13}C NMR (DMSO) δ 166.5, 140.2, 135.1, 134.3, 130.0, 129.6, 127.3, 127.0, 122.6, 120.8, 120.7,
47 119.7, 71.8. ESI-HRMS Cacl.d. for $\text{C}_{17}\text{H}_{14}\text{N}_3\text{O}_4\text{S}$ ($\text{M}-\text{H}^+$): 356.0711; found 356.0706.
48
49
50
51
52
53
54
55
56
57
58
59
60



5: ^1H NMR (500 MHz, DMSO) δ 10.43 (s, 1H), 7.64-7.58 (m, 4H), 7.41 (d, $J = 8.4$ Hz, 2H), 7.30-7.25 (m, 3H), 7.40-7.34 (m, 3H), 4.82 (s, 1H), 3.90 (t, $J = 4.9$ Hz, 4H), 3.43 (s, 4H); ^{13}C NMR (DMSO) δ 166.1, 135.0, 129.9, 127.4, 127.0, 120.0, 71.6, 64.5, 52.8. ESI-HRMS Calcd. for $\text{C}_{18}\text{H}_{19}\text{N}_2\text{O}_5\text{S}$ (M^+): 375.1020; found 375.1020.

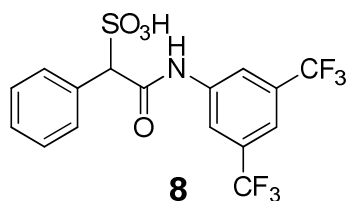


6: ^1H NMR (500 MHz, DMSO) δ 11.05 (s, 1H), 9.29 (d, $J = 2.3$ Hz, 1H), 9.01 (d, $J = 2.1$ Hz, 1H), 8.14 (d, $J = 8.1$ Hz, 1H), 8.07 (d, $J = 8.5$ Hz, 1H), 7.85-7.84 (m, 1H), 7.84-7.82 (m, 1H), 7.76-7.63 (m, 2H), 7.32-7.27 (m, 3H), 4.89 (s, 1H); ^{13}C NMR (DMSO) δ 167.2, 141.3, 138.9, 134.7, 133.3, 130.4, 130.0, 128.6, 128.3, 128.2, 127.4, 127.0, 124.2, 99.5, 71.6. ESI-HRMS Calcd. for $\text{C}_{17}\text{H}_{13}\text{N}_2\text{O}_4\text{S}$ (M^+): 341.0602; found 341.0602.

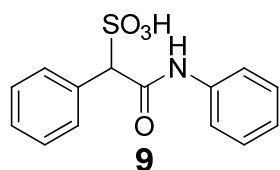


7: ^1H NMR (500 MHz, DMSO) δ 7.97 (d, $J = 7.8$ Hz, 1H), 7.75 (d, $J = 8.0$ Hz, 1H), 7.58 (d, $J = 7.1$ Hz, 2H), 7.43 (t, $J = 7.5$ Hz, 1H), 7.33-7.28 (m, 4H), 5.09 (s, 1H); ^{13}C NMR (DMSO) δ 167.0, 157.6, 148.5,

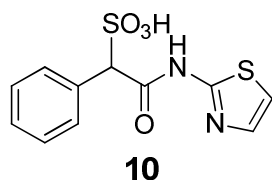
1
2
3 134.3, 131.5, 130.0, 127.6, 127.3, 126.2, 123.6, 121.8, 120.6, 70.3. ESI-HRMS Calcd. for
4
5 C₁₅H₁₁N₂O₄S₂ (M-H⁺): 347.0166; found 347.0166.
6
7



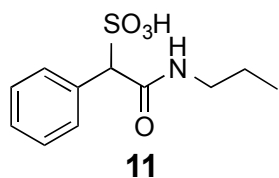
18 **8**: ¹H NMR (500 MHz, DMSO) δ 10.90 (s, 1H), 8.27 (s, 2H), 7.71 (s, 1H), 7.63-7.61(m, 2H), 7.30-7.24
19 (s, 5H), 4.85 (s, 1H); ¹³C NMR (DMSO) δ 167.2, 158.4 (q, *J* = 38.6 Hz), 141.1, 134.6, 130.8 (q, *J* = 32.4
20 Hz), 127.4, 127.1, 123.2 (q, *J* = 271.0 Hz), 120.0, 115.0 (q, *J* = 286.2 Hz), 71.8. ESI-HRMS Calcd. for
21 C₁₆H₁₀F₆NO₄S (M-H⁺): 426.0240; found 426.0237.
22
23
24
25
26
27



37 **9**: ¹H NMR (500 MHz, DMSO) δ 10.23 (s, 1H), 7.56-7.54 (m, 4H), 7.30-7.25 (m, 5H), 7.03 (t, *J* = 7.4
38 Hz, 1H), 4.76 (s, 1H); ¹³C NMR (DMSO) δ 166.2, 139.2, 135.2, 130.1, 129.1, 127.8, 127.4, 123.7,
39 119.3, 72.2. ESI-HRMS Calcd. for C₁₄H₁₃NO₄S (M-H⁺): 292.0638; found 292.0645.
40
41
42
43
44
45

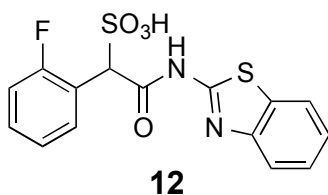


53 **10**: ¹H NMR (500 MHz, DMSO) δ 12.0 (s, 1H), 7.49-7.23 (m, 7H), 4.93 (s, 1H). ESI-HRMS Calcd. for
54 C₁₁H₉N₂O₄S₂ (M-H⁺): 297.0009; found 296.9999.
55
56
57
58
59
60



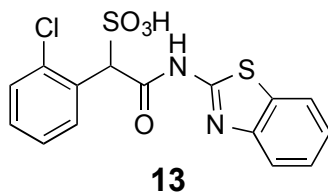
12
13
14
15
16
17
18
19
20
21
22
23

11: ^1H NMR (500 MHz, CDCl_3) δ 8.23 (s, 1H), 7.45-7.44 (m, 2H), 7.27-7.20 (m, 3H), 4.42 (s, 1H), 3.11-3.02 (m, 2 H), 1.46-1.39 (m, 2H), 0.85 (t, $J = 7.4$ Hz, 3H); ^{13}C NMR (500 MHz, CDCl_3) δ 167.3, 135.7, 129.6, 127.4, 126.8, 71.5, 40.4, 22.3, 11.4. ESI-HRMS Calcd. for $\text{C}_{11}\text{H}_{16}\text{NO}_4\text{S}$ ($\text{M}+\text{H}^+$): m/z 258.0795; found 258.0799.



32
33
34
35
36
37
38
39
40
41
42
43
44
45

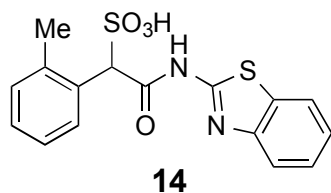
12: ^1H NMR (500 MHz, DMSO) δ 12.43 (s, 1H), 8.08-8.05 (m, 1H), 7.97 (d, $J = 7.9$ Hz, 1H), 7.76 (d, $J = 8.1$ Hz, 1H), 7.45-7.42 (m, 1H), 7.33-7.29 (m, 2H), 7.19-7.12 (m, 2H), 5.46 (s, 1H). ^{13}C NMR (DMSO) δ 166.3, 160.2 (d, $J = 243.9$ Hz, 1H), 157.6, 148.5, 131.9 (d, $J = 3.3$ Hz), 131.5, 129.0 (d, $J = 8.1$ Hz), 126.1, 123.5, 123.4 (d, $J = 3.5$ Hz), 121.7, 121.4 (d, $J = 13.2$ Hz), 114.4 (d, $J = 22.4$ Hz), 61.6. ESI Calcd. for $\text{C}_{15}\text{H}_{10}\text{FN}_2\text{O}_4\text{S}_2$ ($\text{M}-\text{H}^+$): 365.0071; found 365.0081.



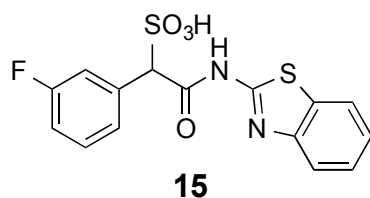
54
55
56
57
58
59
60

13: ^1H NMR (500 MHz, DMSO) δ 8.19 (d, $J = 1.8$ Hz, 1H), 8.18 (d, $J = 1.8$ Hz, 1H), 7.97 (d, $J = 7.9$ Hz, 1H), 7.77-7.41 (m, 2H), 7.35-7.28 (m, 3H), 5.65 (s, 1H). ^{13}C NMR (DMSO) δ 166.2, 157.6, 148.5,

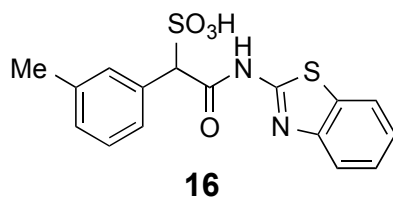
1
2
3 133.9, 132.0, 132.0, 131.5, 128.8, 128.5, 126.2, 126.1, 123.5, 121.7, 120.6, 65.9. ESI Cacl. for
4
5 C₁₅H₁₀CIN₂O₄S₂ (M-H⁺): 380.9776; found 380.9773.
6
7



18 **14:** ¹H NMR (500 MHz, DMSO) δ 12.46 (br, 1H), 7.98-7.96 (m, 2H), 7.75 (d, *J* = 8.1 Hz, 1H), 7.43 (t, *J*
19 = 7.3 Hz, 1H), 7.30 (t, *J* = 7.3 Hz, 1H), 7.15-7.14 (m, 3H), 5.34 (s, 1H). ¹³C NMR (DMSO) δ 167.1,
20 157.7, 148.5, 137.1, 132.7, 131.4, 129.6, 129.5, 126.9, 126.1, 125.0, 123.5, 121.7, 120.5, 65.7, 19.8. ESI
21 Cacl. for C₁₆H₁₃N₂O₄S₂ (M-H⁺): 361.0322; found 361.0328.
22
23
24
25
26
27

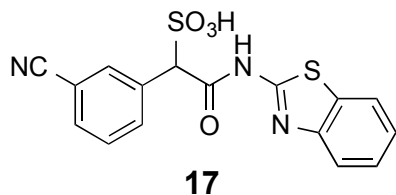


37 **15:** ¹H NMR (500 MHz, DMSO) δ 12.28 (s, 1H), 7.98 (d, *J* = 7.7 Hz, 1H), 7.76 (d, *J* = 7.9 Hz, 1H), 7.51
38 (d, *J* = 10.0 Hz, 1H), 7.43 (t, *J* = 7.4 Hz, 1H), 7.35-7.29 (m, 3H), 7.12 (t, *J* = 7.1 Hz, 1H), 5.15 (s, 1H);
39
40 ¹³C NMR (DMSO) δ 166.6, 161.5 (d, *J* = 240.0 Hz, 1H), 157.5, 148.5, 136.9 (d, *J* = 7.9 Hz), 131.5,
41 129.2 (d, *J* = 7.9 Hz), 126.2, 126.1, 123.5, 121.7, 120.6, 116.5 (d, *J* = 22.3 Hz), 114.0 (d, *J* = 21.0 Hz),
42 69.6. ESI-HRMS Cacl. for C₁₅H₁₀FN₂O₄S₂ (M-H⁺): 365.0071; found 365.0071.
43
44
45
46
47
48
49
50

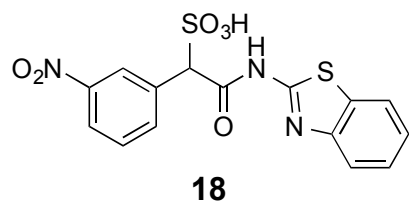


1
2
3
4
5
6
7
8
9
10
11
12
13
14
15
16
17
18
19
20
21
22
23
24
25
26
27
28
29
30
31
32
33
34
35
36
37
38
39
40
41
42
43
44
45
46
47
48
49
50
51
52
53
54
55
56
57
58
59
60

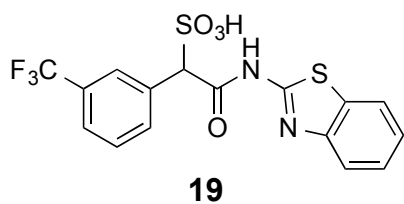
16: ^1H NMR (500 MHz, DMSO) δ 7.97 (d, $J = 7.9$ Hz, 1H), 7.75 (d, $J = 8.1$ Hz, 1H), 7.45-7.36 (m, 3H), 7.30 (t, $J = 7.6$ Hz, 1H), 7.19 (t, $J = 7.6$ Hz, 1H), 7.09 (d, $J = 7.4$ Hz, 1H), 5.02 (s, 1H), 2.30 (s, 3H). ^{13}C NMR (DMSO) δ 167.7, 157.5, 148.4, 136.4, 134.2, 131.4, 130.4, 127.9, 127.5, 127.0, 126.1, 123.5, 121.7, 120.5, 70.3, 21.1. ESI Calcd. for $\text{C}_{16}\text{H}_{13}\text{N}_2\text{O}_4\text{S}_2$ ($\text{M}-\text{H}^+$): 361.0322; found 361.0333.



17: ^1H NMR (500 MHz, DMSO) δ 8.06 (s, 1H), 7.98 (d, $J = 7.8$ Hz, 1H), 7.84 (d, $J = 7.9$ Hz, 1H), 7.78-7.75 (m, 2H), 7.55 (t, $J = 7.8$ Hz, 1H), 7.44 (t, $J = 7.3$ Hz, 1H), 7.31 (d, $J = 7.4$ Hz, 1H), 5.25 (s, 1H). ^{13}C NMR (DMSO) δ 166.4, 157.5, 148.5, 135.9, 135.1, 133.4, 131.5, 130.9, 128.9, 126.2, 123.6, 121.7, 120.6, 118.9, 110.5, 69.3. ESI Calcd. for $\text{C}_{16}\text{H}_{10}\text{N}_3\text{O}_4\text{S}_2$ ($\text{M}-\text{H}^+$): 372.0118; found 372.0129.

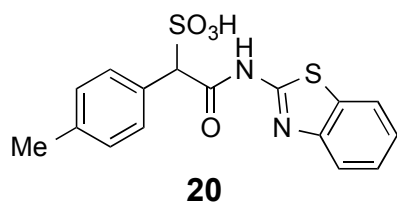


18: ^1H NMR (500 MHz, DMSO) δ 8.58 (s, 1H), 8.18 (d, $J = 8.0$ Hz, 1H), 7.99-7.94 (m, 2H), 7.77 (d, $J = 8.1$ Hz, 1H), 7.63 (t, $J = 7.9$ Hz, 1H), 7.44 (t, $J = 7.4$ Hz, 1H), 7.31 (d, $J = 7.4$ Hz, 1H), 5.37 (s, 1H). ^{13}C NMR (DMSO) δ 166.3, 157.5, 148.5, 147.2, 137.0, 136.4, 131.5, 129.0, 126.2, 124.6, 123.6, 122.2, 121.7, 120.6, 69.2. ESI Calcd. for $\text{C}_{15}\text{H}_{10}\text{N}_3\text{O}_6\text{S}_2$ ($\text{M}-\text{H}^+$): 392.0017; found 392.0026.



10
11
12
13
14
15
16
17
18
19
20
21
22
23
24

19: ^1H NMR (500 MHz, DMSO) δ 8.03 (s, 1H), 7.97 (d, $J = 7.9$ Hz, 1H), 7.81 (d, $J = 7.6$ Hz, 1H), 7.76 (d, $J = 8.1$ Hz, 1H), 7.65 (d, $J = 7.7$ Hz, 1H), 7.56 (t, $J = 7.7$ Hz, 1H), 7.43 (t, $J = 7.6$ Hz, 1H), 7.30 (d, $J = 7.6$ Hz, 1H), 5.29 (s, 1H). ^{13}C NMR (125 MHz, DMSO) δ 166.5, 157.5, 148.5, 135.6, 134.2, 131.5, 128.6, 128.3 (q, $J = 31.0$ Hz), 126.4 (d, $J = 3.6$ Hz), 126.2, 124.4 (q, $J = 270.4$ Hz), 124.0 (d, $J = 3.4$ Hz), 123.6, 121.7, 120.6, 69.6. ESI Calcd. for $\text{C}_{16}\text{H}_{10}\text{F}_3\text{N}_2\text{O}_4\text{S}_2$ ($\text{M}-\text{H}^+$): 415.0040; found 415.0046.



33
34
35
36
37
38
39
40
41
42
43
44

20: ^1H NMR (500 MHz, DMSO) δ 7.97 (d, $J = 7.8$ Hz, 1H), 7.75 (d, $J = 8.1$ Hz, 1H), 7.47-7.42 (m, 3H), 7.30 (t, $J = 7.6$ Hz, 1H), 7.11 (d, $J = 7.8$ Hz, 2H), 5.02 (s, 1H), 2.28 (s, 3H). ^{13}C NMR (DMSO) δ 167.2, 157.6, 148.4, 136.4, 131.4, 131.3, 129.7, 128.1, 126.1, 123.5, 121.7, 120.5, 70.0, 20.7. ESI Calcd. for $\text{C}_{16}\text{H}_{13}\text{N}_2\text{O}_4\text{S}_2$ ($\text{M}-\text{H}^+$): 361.0322; found 361.0330.

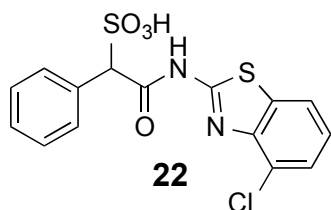


52
53
54
55
56
57
58
59
60

21: ^1H NMR (500 MHz, DMSO) δ 12.28 (s, 1H), 7.97 (d, $J = 7.7$ Hz, 1H), 7.75 (d, $J = 8.0$ Hz, 1H), 7.55-7.50 (m, 4H), 7.43 (t, $J = 7.5$ Hz, 1H), 7.30 (d, $J = 7.4$ Hz, 1H), 5.12 (s, 1H); ^{13}C NMR (DMSO) δ

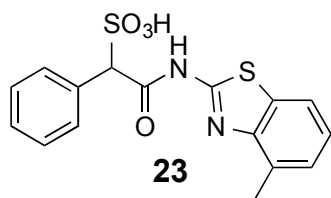
1
2
3 166.6, 157.5, 148.5, 133.7, 132.1, 131.5, 130.4, 126.1, 123.5, 121.7, 120.6, 120.6, 69.5. ESI-HRMS

4
5
6 Cacl. for C₁₅H₁₀BrN₂O₄S₂ (M-H⁺): 424.9271; found 424.9270.



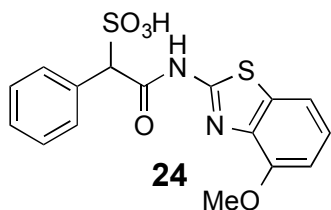
18 **22:** ¹H NMR (500 MHz, DMSO) δ 12.57 (s, 1H), 7.92-7.25 (m, 8H), 5.04 (s, 1H). ESI-HRMS Cacl. for

19
20 C₁₅H₁₀ClN₂O₄S₂ (M-H⁺): 380.9776; found 380.9777.



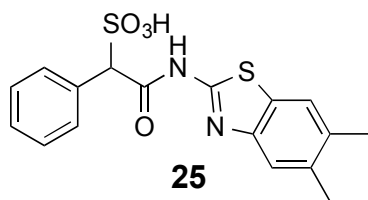
33 **23:** ¹H NMR (500 MHz, DMSO) δ 12.32 (s, 1H), 7.77-7.24 (m, 8H), 5.07 (s, 1H). ESI-HRMS Cacl. for

34
35 C₁₆H₁₃N₂O₄S₂ (M-H⁺): 361.0322; found 361.0316.



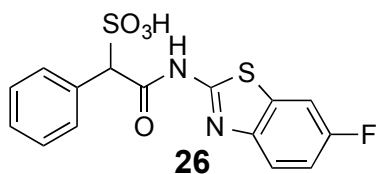
48 **24:** ¹H NMR (500 MHz, DMSO) δ 12.40 (br, 1H), 7.59-6.98 (m, 8H), 5.10 (s, 1H), 3.91 (br, 3H). ESI-

49
50 HRMS Cacl. for C₁₆H₁₃N₂O₅S₂ (M-H⁺): 377.0271; found 377.0266.



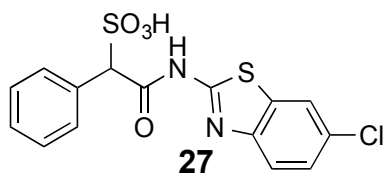
10
11
12
13
14
15
16
17

25: ^1H NMR (500 MHz, DMSO) δ 12.24 (br, 1H), 7.99-7.29 (m, 7H), 4.94 (s, 1H), 2.30 (6H). ESI-HRMS Calcd. for $\text{C}_{17}\text{H}_{15}\text{N}_2\text{O}_4\text{S}_2$ ($\text{M}-\text{H}^+$): 375.0479; found 375.0473.



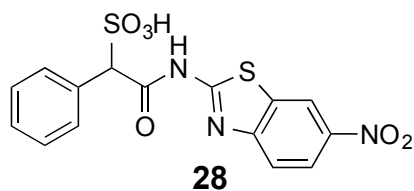
25
26
27
28
29
30
31

26: ^1H NMR (500 MHz, DMSO) δ 12.35 (br, 1H), 7.88-7.28 (m, 8H), 5.07 (s, 1H). ESI-HRMS Calcd. for $\text{C}_{15}\text{H}_{10}\text{FN}_2\text{O}_4\text{S}_2$ ($\text{M}-\text{H}^+$): m/z 365.0071; found 365.0071.



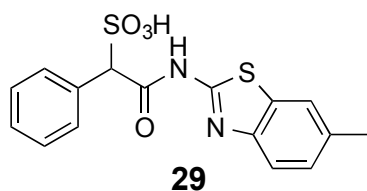
39
40
41
42
43
44
45

27: ^1H NMR (500 MHz, DMSO) δ 12.35 (br, 1H), 8.10 (s, 1H), 7.72-7.27 (m, 7H), 5.05 (s, 1H). ESI-HRMS Calcd. for $\text{C}_{15}\text{H}_{10}\text{ClN}_2\text{O}_4\text{S}_2$ ($\text{M}-\text{H}^+$): 380.9776; found 380.9768.



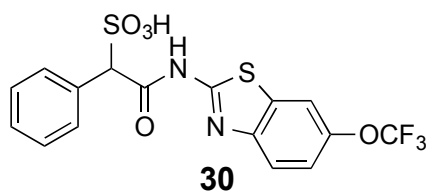
53
54
55
56
57
58
59
60

28: ^1H NMR (500 MHz, DMSO) δ 12.64 (s, 1H), 9.00 (s, 1H), 8.21-7.24 (m, 7H), 5.09 (s, 1H). ESI-HRMS Calcd. for $\text{C}_{15}\text{H}_{10}\text{N}_3\text{O}_6\text{S}_2$ ($\text{M}-\text{H}^+$): 392.0017; found 392.0014.



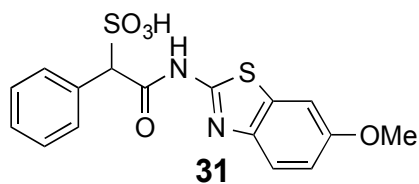
13
14
15
16
17
18
19

29: ^1H NMR (500 MHz, DMSO) δ 12.16 (s, 1H), 7.70-7.23 (m, 8H), 5.00 (s, 1H), 2.35 (s, 3H). ESI-HRMS Calcd. for $\text{C}_{16}\text{H}_{13}\text{N}_2\text{O}_4\text{S}_2$ ($\text{M}-\text{H}^+$): 361.0322; found 361.0315.



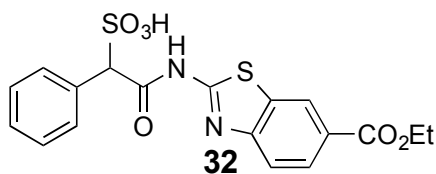
27
28
29
30
31
32

30: ^1H NMR (500 MHz, DMSO) δ 12.35 (s, 1H), 8.05-7.25 (m, 8H), 5.04 (s, 1H). ESI-HRMS Calcd. for $\text{C}_{16}\text{H}_{10}\text{F}_3\text{N}_2\text{O}_5\text{S}_2$ ($\text{M}-\text{H}^+$): 430.9989; found 430.9993.



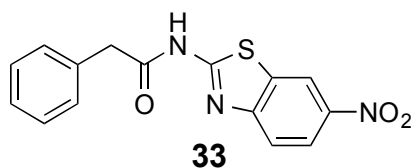
42
43
44
45
46
47

31: ^1H NMR (500 MHz, DMSO) δ 12.05 (s, 1H), 7.49-6.93 (m, 8H), 4.94 (s, 1H), 3.70 (s, 3H). ESI-HRMS Calcd. for $\text{C}_{16}\text{H}_{13}\text{N}_2\text{O}_5\text{S}_2$ ($\text{M}-\text{H}^+$): 377.0271; found 377.0268.



1
2
3
4
5
6
7
8
9
10
11
12
13
14
15
16
17
18
19
20
21
22
23
24
25
26
27
28
29
30
31
32
33
34
35
36
37
38
39
40
41
42
43
44
45
46
47
48
49
50
51
52
53
54
55
56
57
58
59
60

32: ^1H NMR (500 MHz, DMSO) δ 12.47 (s, 1H), 8.59 (s, 1H), 7.95-7.25 (m, 8H), 5.10 (s, 1H), 4.26 (br, 2H), 1.27 (br, 3H). ESI-HRMS Calcd. for $\text{C}_{18}\text{H}_{15}\text{N}_2\text{O}_6\text{S}_2$ ($\text{M}-\text{H}^+$): 419.0377; found 419.0374.



33: ^1H NMR (500 MHz, DMSO) δ 8.70 (d, $J = 2.3$ Hz, 1H), 8.26 (dd, $J = 2.4, 9.0$ Hz, 1H), 7.73 (d, $J = 9.0$ Hz, 1H), 7.38-7.31 (m, 5H); ^{13}C NMR (DMSO) 170.1, 162.4, 153.0, 143.9, 132.5, 129.4, 129.3, 128.0, 121.9, 120.7, 118.1, 43.2. ESI-HRMS Calcd. for $\text{C}_{15}\text{H}_{10}\text{N}_3\text{O}_3\text{S}$ ($\text{M}-\text{H}^+$): 312.0448; found 312.0444.

Protein Expression and Purification. Expression and purification of the His-tagged LMW-PTP isoform A was performed as described elsewhere.³⁹ LMW-PTPA was expressed in BL21 *E. coli* cells. Protein expression was induced by 0.6 mM IPTG and harvested after overnight incubation at 25 °C. The cells were pelleted by centrifugation at 5,000 rpm and resuspended in 30 ml of 100 mM Tris buffer, pH 7.8, with 500 mM NaCl and 10 mM imidazole. The suspensions were frozen and thawed before physical lysis by a French Press. The bacterial lysate was centrifuged at 15,000 rpm at 4 °C for 30 min. The supernatant was collected and incubated with 2 ml of Ni-NTA resin by end-over-end rotation for 1 h at 4 °C. The beads were washed with the same Tris buffer with 20 mM imidazole to remove nonspecific binding. LMWPTP was eluted with 250 mM imidazole in the same Tris buffer. The protein was concentrated and further purified by going through a Sephadex G75 column. The other PTPs for selectivity studies were expressed and purified from *E. coli* by the same method used for LMW-PTP. These PTPs included SHP2, PTP1B, TC-PTP, SHP1, LYP, HePTP, Meg2, PTPH1, FAP-1, PTP-PEST, CD45, LAR, PTP α , PTP β , PTP γ , PTP ϵ , PTP σ , PTP μ , MKP3, VHR, VHZ, CDC14A, SSu72, and PP5.

1
2
3
4
5
6
7
8
9
10
11
12
13
14
15
16
17
18
19
20
21
22
23
24
25
26
27
28
29
30
31
32
33
34
35
36
37
38
39
40
41
42
43
44
45
46
47
48
49
50
51
52
53
54
55
56
57
58
59
60

Crystallization, Data Collection, and Structure Determination. Protein crystals were first grown in 100 mM MES buffer, 30% PEGME 5,000 and 0.2 M Ammonium sulfate, the same buffer used elsewhere³⁹ in the presence of 1 mM compound 7. Crystallization conditions were systematically scanned against a number of different buffers instead of MES and eventually the optimal condition was finalized for crystal growth of the LMWPTP•7 complex. The buffer grid is 25-30% PEGME 5,000 in 100 mM Bis-Tris, pH 6.0-6.5. The data was collected at the APS 19BM or 19ID beamlines (Argonne, IL). Initial phases of the LMWPTP complexes were determined by molecular replacement with the CCP4 software package. The published LMWPTP structure (5PNT) was used as the initial search model. After one round of refinement by Refmac in the CCP4 package, further refinement was carried out in Phenix.

Determination of Inhibition Constant and IC₅₀. PTP activity was measured using p-nitrophenyl phosphate (pNPP) as a substrate in 50 mM 3,3-dimethylglutarate (DMG) buffer, pH 7.0 at 25 °C. The reaction was initiated by the addition of enzyme to a reaction solution containing 2-5 mM pNPP with different concentrations of inhibitors. The reactions were incubated at room temperature for 5-10 min and quenched with 5N NaOH. The nonenzymatic hydrolysis of pNPP was corrected by measuring the control without the addition of enzyme. The amount of product p-nitrophenol was determined from the absorbance at 405 nm detected by a Spectra MAX340 microplate spectrophotometer (Molecular Devices) using a molar extinction coefficient of 18,000 M⁻¹cm⁻¹. IC₅₀ was calculated by fitting the data using SigmaPlot. To determine the mode of inhibition, the reactions were initiated by addition of enzyme to the reaction solution containing different concentrations of pNPP with different concentrations of inhibitor. Similarly, K_i was obtained by fitting the data using SigmaPlot Enzyme Kinetics Module. In addition to LMW-PTP, other PTPs evaluated included the receptor-like PTPs, CD45, PTP α , PTP β , PTP μ , PTP ϵ , LAR, PTP σ and PTP γ , cytosolic PTPs, PTP1B, TC-PTP, Lyp, SHP1,

1
2
3 SHP2, PTPH1, HePTP, PTP-Meg2, PTP-FAP1, and PTP-PEST, the dual specificity phosphatase VHR,
4
5 VHZ, MKP3, CDC14A, RNA Polymerase II CTD Phosphatase, and protein phosphatase 5. The IC₅₀
6
7
8 determination for these PTPs was performed under the same conditions as used for LMW-PTP except
9
10 that the pNPP concentrations used corresponded to the K_m values of the PTPs studied and the enzyme
11
12 concentrations ranged from 5-20 nM.
13
14

15
16 *Cell culture and immunoblot analysis.* HepG2 cells were cultured at 37 °C and 5% CO₂ in
17
18 Dulbecco's modified Eagle's medium (Corning) supplemented with 10% fetal bovine serum (HyClone).
19
20 The 60-80% confluent HepG2 cells were starved overnight in serum free medium, followed by
21
22 treatment with vehicle or compound for 2h, and then either left unstimulated or stimulated with 50 nM
23
24 insulin (Sigma) for 30 min. Cells were lysed and the lysates were electrophoresed on a 10%
25
26 polyacrylamide gel, transferred to a nitrocellulose membrane, and blotted with anti-phospho-AKT, anti-
27
28 AKT antibodies (Cell Signaling). The blots were developed by the enhanced chemiluminescence
29
30 technique using the SuperSignal West Pico Chemiluminescent substrate (Thermo Scientific). The
31
32 protein levels of phospho-AKT and AKT were quantified by Image J software, and the ratios of
33
34 pAKT/AKT were normalized to the vehicle control.
35
36
37
38
39
40
41
42
43

44 **Acknowledgement:** This work was supported in part by National Institutes of Health Grants CA69202
45
46 and P30CA023168.
47
48
49
50
51

52 **Ancillary Information**

53
54
55 *Data deposition:* The coordinates for the structures of LMW-PTP•7 (accession number 5KQG), LMW-
56
57 PTP•9 (accession number 5KQL), LMW-PTP•MES (accession number 5KQM), and the apo-form
58
59
60

1
2
3 LMW-PTP (accession number 5KQP) have been deposited in the Protein Data Bank. Authors will
4
5 release the atomic coordinates and experimental data upon article publication.
6
7
8
9

10 *To whom correspondence should be addressed. Phone: (765) 494-1403; E-mail: zhang-zy@purdue.edu
11

12 #These authors contributed equally to the work.
13
14
15
16
17

18 *Abbreviations footnote:* LMW-PTP, low molecular weight protein tyrosine phosphatase; PTP, protein
19
20 tyrosine phosphatase; SPAA, SulfoPhenyl Acetic Amide.
21
22
23
24
25
26
27
28
29
30
31
32
33
34
35
36
37
38
39
40
41
42
43
44
45
46
47
48
49
50
51
52
53
54
55
56
57
58
59
60

References

1. Hunter, T. Tyrosine phosphorylation: thirty years and counting. *Curr. Opin. Cell Biol.* **2009**, *21*, 140-146.
2. He, R.; Yu, Z.-H.; Zhang, R.-Y.; Zhang, Z.-Y. Protein tyrosine phosphatases as potential therapeutic targets. *Acta Pharmacol. Sin.* **2014**, *35*, 1227-1246.
3. Cohen, P.; Alessi, D. R. Kinase drug discovery - what's next in the field? *ACS Chem. Biol.* **2013**, *8*, 96-104.
4. Alonso, A.; Sasin, J.; Bottini, N.; Friedberg, I.; Friedberg, I.; Osterman, A.; Godzik, A.; Hunter, T.; Dixon, J.; Mustelin, T. Protein tyrosine phosphatases in the human genome. *Cell* **2004**, *117*, 699-711.
5. Zhang, Z.-Y.; Van Etten, R. L. Purification and characterization of a low-molecular-weight acid phosphatase--a phosphotyrosyl-protein phosphatase from bovine heart. *Arch. Biochem. Biophys.* **1990**, *282*, 39-49.
6. Wang, S.; Taberero, L.; Zhang, M.; Harms, E.; Van Etten, R.L.; Stauffacher, C.V. Crystal structures of a low-molecular weight protein tyrosine phosphatase from *Saccharomyces cerevisiae* and its complex with the substrate p-nitrophenyl phosphate. *Biochemistry* **2000**, *39*, 1903-1914.
7. Tolkatchev, D.; Shaykhtudinov, R.; Xu, P.; Plamondon, J.; Watson, D.C.; Young, N.M.; Ni, F. Three-dimensional structure and ligand interactions of the low molecular weight protein tyrosine phosphatase from *Campylobacter jejuni*. *Protein Science* **2006**, *15*, 2381-2394.
8. Maccari, R.; Ottanà, R. Low molecular weight phosphotyrosine protein phosphatases as emerging targets for the design of novel therapeutic agents. *J. Med. Chem.* **2012**, *55*, 2-22.
9. Chiarugi, P.; Cirri, P.; Taddei, M.L.; Giannoni, E.; Fiaschi, T.; Buricchi, F.; Camici, G.; Raugei, G.; Ramponi, G. Insight into the role of low molecular weight phosphotyrosine phosphatase (LMW-

- 1
2
3 PTP) on platelet-derived growth factor receptor (PDGF-r) signaling. LMW-PTP controls PDGF-
4 r kinase activity through TYR-857 dephosphorylation. *J. Biol. Chem.* **2002**, *277*, 37331–37338.
5
6
7
8 10. Taddei, M.L.; Chiarugi, P.; Cirri, P.; Talini, D.; Camici, G.; Manao, G.; Raugei, G.; Ramponi, G.
9
10 LMW-PTP exerts a differential regulation on PDGF- and insulin-mediated signaling. *Biochem.*
11
12 *Biophys. Res. Commun.* **2000**, *270*, 564–569.
13
14
15 11. Shimizu, H.; Shiota, M.; Yamada, N.; Miyazaki, K.; Ishida, N.; Kim, S.; Miyazaki, H. Low M(r)
16
17 protein tyrosine phosphatase inhibits growth and migration of vascular smooth muscle cells
18
19 induced by platelet-derived growth factor. *Biochem. Biophys. Res. Commun.* **2001**, *289*, 602–
20
21 607.
22
23
24 12. Park, E.K.; Warner, N.; Mood, K.; Pawson, T.; Daar, I.O. Low-molecular-weight protein tyrosine
25
26 phosphatase is a positive component of the fibroblast growth factor receptor signaling pathway.
27
28 *Mol. Cell. Biol.* **2002**, *22*, 3404–3414.
29
30
31 13. Ramponi, G.; Manao, G.; Camici, G.; Cappugi, G.; Ruggiero, M.; Bottaro, D.P. The 18 kDa
32
33 cytosolic acid phosphatase from bovine liver has phosphotyrosine phosphatase activity on the
34
35 autophosphorylated epidermal growth factor receptor. *FEBS Lett.* **1989**, *250*, 469–473.
36
37
38 14. Chiarugi, P.; Cirri, P.; Marra, F.; Raugei, G.; Camici, G.; Manao, G.; Ramponi, G. LMW-PTP is a
39
40 negative regulator of insulin-mediated mitotic and metabolic signalling. *Biochem. Biophys. Res.*
41
42 *Commun.* **1997**, *238*, 676–682.
43
44
45 15. Pandey, S.K.; Yu, X.X.; Watts, L.M.; Michael, M.D.; Sloop, K.W.; Rivard, A.R.; Leedom, T.A.;
46
47 Mancham, V.P.; Samadzadeh, L.; McKay, R.A.; Monia, B.P.; Bhanot, S. Reduction of low
48
49 molecular weight protein-tyrosine phosphatase expression improves hyperglycemia and insulin
50
51 sensitivity in obese mice. *J. Biol. Chem.* **2007**, *282*, 14291–14299.
52
53
54
55
56
57
58
59
60

- 1
2
3
4 16. Chiarugi, P.; Pani, G.; Giannoni, E.; Taddei, L.; Colavitti, R.; Raugei, G.; Symons, M.; Borrello, S.;
5
6 Galeotti, T.; Ramponi, G. Reactive oxygen species as essential mediators of cell adhesion: the
7
8 oxidative inhibition of a FAK tyrosine phosphatase is required for cell adhesion. *J. Cell Biol.*
9
10 **2003**, *161*, 933–944.
11
- 12
13 17. Swanson, P.A.; Kumar, A.; Samarin, S.; Vijay-Kumar, M.; Kundu, K.; Murthy, N.; Hansen, J.;
14
15 Nusrat, A.; Neish, A.S. Enteric commensal bacteria potentiate epithelial restitution via reactive
16
17 oxygen species-mediated inactivation of focal adhesion kinase phosphatases. *Proc. Natl. Acad.*
18
19 *Sci. USA.* **2011**, *108*, 8803-8808.
20
21
- 22 18. Rigacci, S.; Talini, D.; Berti, A. LMW-PTP associates and dephosphorylates STAT5 interacting with
23
24 its C-terminal domain. *Biochem. Biophys. Res. Commun.* **2003**, *312*, 360–366.
25
26
- 27 19. Rigacci, S.; Guidotti, V.; Parri, M.; Berti, A. Modulation of STAT5 interaction with LMW-PTP
28
29 during early megakaryocyte differentiation. *Biochemistry* **2008**, *47*, 1482–1489.
30
31
- 32 20. Stein, E.; Lane, A.A.; Cerretti, D.P.; Schoecklmann, H.O.; Schroff, A.D.; Van Etten, R.L.; Daniel,
33
34 T.O. Eph receptors discriminate specific ligand oligomers to determine alternative signaling
35
36 complexes, attachment, and assembly responses. *Genes Dev.* **1998**, *12*, 667–678.
37
38
- 39 21. Kikawa, K.D.; Vidale, D.R.; Van Etten, R.L.; Kinch, M.S. Regulation of the EphA2 kinase by the
40
41 low molecular weight tyrosine phosphatase induces transformation. *J. Biol. Chem.* **2002**, *277*,
42
43 39274–39279.
44
45
- 46 22. Malentacchi, F.; Marzocchini, R.; Gelmini, S.; Orlando, C.; Serio, M.; Ramponi, G.; Raugei, G. Up-
47
48 regulated expression of low molecular weight protein tyrosine phosphatases in different human
49
50 cancers. *Biochem. Biophys. Res. Commun.* **2005**, *334*, 875–883.
51
52
53
54
55
56
57
58
59
60

- 1
2
3
4
5
6
7
8
9
10
11
12
13
14
15
16
17
18
19
20
21
22
23
24
25
26
27
28
29
30
31
32
33
34
35
36
37
38
39
40
41
42
43
44
45
46
47
48
49
50
51
52
53
54
55
56
57
58
59
60
23. Marzocchini, R.; Malentacchi, F.; Biagini, M.; Cirelli, D.; Luceri, C.; Caderni, G.; Raugei, G. The expression of low molecular weight protein tyrosine phosphatase is up-regulated in 1,2-dimethylhydrazine-induced colon tumours in rats. *Int J Cancer* **2007**, *122*, 1675–1678.
24. Ruela-de-Sousa, R.R.; Hoekstra, E.; Hoogland, A.M.; Souza Queiroz, K. C.; Peppelenbosch, M.P.; Stubbs, A.P.; Pelizzaro-Rocha, K.; van Leenders, G.J.; Jenster, G.; Aoyama, H.; Ferreira, C.V.; Fuhler, G.M. Low-molecular-weight protein tyrosine phosphatase predicts prostate cancer outcome by increasing the metastatic potential. *Eur Urol.* **2016**, *69*, 710-719
25. Hoekstra, E.; Kodach, L.L.; Das, A.M.; Ruela-de-Sousa, R.R.; Ferreira, C.V.; Hardwick, J.C.; van der Woude, C.J.; Peppelenbosch, M.P.; Ten Hagen, T.L.; Fuhler, G.M. Low molecular weight protein tyrosine phosphatase (LMWPTP) upregulation mediates malignant potential in colorectal cancer. *Oncotarget* **2015**, *6*, 8300-8312.
26. Bottini, N.; MacMurray, J.; Peters, W.; Rostamkhani, M.; Comings, D.E. Association of the acid phosphatase (ACP1) gene with triglyceride levels in obese women. *Molecular Genetics and Metabolism* **2002**, *77*, 226–229.
27. Iannaccone, U.; Bergamaschi, A.; Magrini, A.; Marino, G.; Bottini, N.; Lucarelli, P.; Bottini, E.; Gloria-Bottini, F. Serum glucose concentration and ACP1 genotype in healthy adult subjects. *Metab. Clin. Exp.* **2005**, *54*, 891–894.
28. Gloria-Bottini, F.; Magrini, A.; Renzo, L.D.; Lorenzo, A.D.; Bergamaschi, A.; Bottini, E. Body mass index and acid phosphatase locus 1 in diabetic disorders. *Acta Diabetol* **2010**, *47*, 139–143.
29. Zabell, A. P.; Corden, S.; Helquist, P.; Stauffacher, C. V.; Wiest, O. Inhibition studies with rationally designed inhibitors of the human low molecular weight protein tyrosine phosphatase. *Bioorg. Med. Chem.* **2004**, *12*, 1867-1880.

- 1
2
3
4 30. Weitgenant, J. A.; Katsuyama, I.; Bigi, M. A.; Corden, S. J.; Markiewicz, J. T.; Zabell, A. P. R.;
5
6 Homan, K. T.; Wiest, O.; Stauffacher, C. V.; Helquist, P. Synthesis of a 5-azaindole phosphonic
7
8 acid as a computationally designed inhibitor of the low molecular weight phosphatase HCPTP.
9
10 *Heterocycles* **2006**, *70*, 599-607.
11
- 12
13 31. Vidal, D.; Blobel, J.; Pérez, Y.; Thormann, M.; Pons, M. Structure-based discovery of new small
14
15 molecule inhibitors of low molecular weight protein tyrosine phosphatase. *Eur. J. Med. Chem.*
16
17 **2007**, *42*, 1102–1108.
18
- 19
20 32. Maccari, R.; Ottanà, R.; Ciurleo, R.; Paoli, P.; Manao, G.; Camici, G.; Laggner, C.; Langer, T.
21
22 Structure-based optimization of benzoic acids as inhibitors of protein tyrosine phosphatase 1B
23
24 and low molecular weight protein tyrosine phosphatase. *ChemMedChem* **2009**, *4*, 957–962.
25
26
- 27 33. Ottanà, R.; Maccari, R.; Ciurleo, R.; Paoli, P.; Jacomelli, M.; Manao, G.; Camici, G.; Laggner, C.;
28
29 Langer, T. 5-Arylidene-2-phenylimino-4-thiazolidinones as PTP1B and LMW-PTP inhibitors.
30
31 *Bioorg. Med. Chem.* **2009**, *17*, 1928–1937.
32
33
- 34 34. Homan, K.T.; Balasubramaniam, D.; Zabell, A.P.R.; Wiest, O.; Helquist, P.; Stauffacher, C.V.
35
36 Identification of novel inhibitors for a low molecular weight protein tyrosine phosphatase via
37
38 virtual screening. *Bioorg. Med. Chem.* **2010**, *18*, 5449–5456.
39
40
- 41 35. Forghieri, M.; Laggner, C.; Paoli, P.; Langer, T.; Manao, G.; Camici, G.; Bondioli, L.; Prati, F.;
42
43 Costantino, L. Synthesis, activity and molecular modeling of a new series of chromones as low
44
45 molecular weight protein tyrosine phosphatase inhibitors. *Bioorg. Med. Chem.* **2009**, *17*, 2658–
46
47 2672.
48
49
- 50 36. Seiler, C. L.; Richards, K. A.; Jakubowski, H. V.; McIntee, E. J. Identification of new inhibitors for
51
52 low molecular weight protein tyrosine phosphatase isoform B. *Bioorg. Med. Chem. Lett.* **2013**,
53
54 *23*, 5912-5914
55
56
57
58
59
60

- 1
2
3
4
5
6
7
8
9
10
11
12
13
14
15
16
17
18
19
20
21
22
23
24
25
26
27
28
29
30
31
32
33
34
35
36
37
38
39
40
41
42
43
44
45
46
47
48
49
50
51
52
53
54
55
56
57
58
59
60
37. Ottanà, R.; Maccari, R.; Amuso, S.; Wolber, G.; Schuster, D.; Herdlinger, S.; Manao, G.; Camici, G.; Paoli, P. New 4-[(5-arylidene-2-arylimino-4-oxo-3-thiazolidinyl)methyl]benzoic acids active as protein tyrosine phosphatase inhibitors endowed with insulinomimetic effect on mouse C2C12 skeletal muscle cells. *Eur. J. Med. Chem.* **2012**, *50*, 332–343.
38. He, R.; Yu, Z.-H.; Zhang, R.-Y.; Wu, L.; Gunawan, A.; Lane, B. S.; Shim, J. S.; Zeng, L.-F.; He, Y.; Chen, L.; Wells, C. D.; Liu, J. O.; Zhang, Z.-Y. Exploring the existing drug space for novel pTyr mimetic and SHP2 inhibitors. *ACS Medicinal Chemistry Letter* **2015**, *6*, 782-786.
39. Zhang, M.; Stauffacher, C.V.; Lin, D.; Van Etten, R.L. Crystal structure of a human low molecular weight phosphotyrosyl phosphatase. Implications for substrate specificity. *J. Biol. Chem.* **1998**, *273*, 21714–21720.
40. Burley, S.K.; Petsko, G.A. Aromatic-aromatic interaction: a mechanism of protein structure stabilization. *Science* **1985**, *229*, 23–28.
41. Burley, S.K.; Petsko, G.A. Amino-aromatic interactions in proteins. *FEBS Lett.* **1986**, *203*, 139–143.
42. McGaughey, G.B.; Gagné, M.; Rappé, A.K. pi-Stacking interactions. Alive and well in proteins. *J. Biol. Chem.* **1998**, *273*, 15458-15463.
43. Riley, K.E.; Hobza, P. On the importance and origin of aromatic interactions in chemistry and biodisciplines. *Acc. Chem. Res.* **2013**, *46*, 927-936.

Figure Legends

Figure 1 Structure and activity of SPAA-based LMW-PTP inhibitors.

Figure 2. Lineveaver-Burk plot for compound **7** mediated LMW-PTP inhibition at five different concentrations (0 (●), 5 (μ), 10 (τ), 15 (∇), and 20 (■) μM). pNPP was used as the substrate. The data show that compound **7** inhibits the LMW-PTP catalyzed pNPP hydrolysis in a competitive manner ($K_i = 3.2 \pm 0.1 \mu\text{M}$).

Figure 3. Small molecule ligand or water is identified at the active site of LMW-PTP. Unbiased Fo-Fc difference map of (A) MES, (B) Compound **7**, (C) Compound **9**, and (D) three waters contoured at +3σ level is shown in green mesh. Small molecules are shown in stick (carbon in cyan), waters are shown in sphere, and the catalytic Cys12 and Arg18 in LMW-PTP are shown in stick (carbon in gray).

Figure 4. Compound **7** or **9** binding with LMW-PTP induces localized conformation changes leading to the formation of a new hydrophobic cavity within active site pocket. The structure superimposition of (A) LMW-PTP•MES (yellow) with LMW-PTP•**7** (green), (B) LMW-PTP•MES (yellow) with LMW-PTP apo (gray), (C) LMW-PTP•**7** (yellow) with LMW-PTP•**9** (cyan) was performed, the small molecules are shown in thin stick, and local conformation around active site is shown in ribbon diagram with p-loop residues shown in stick. (D) New hydrophobic cavity induced by Compound **7** (carbon in green) or **9** (carbon in cyan) binding accommodates the α-phenyl ring in compound **7** or **9** very well. Residues constituting the cavity are shown in stick underneath the surface.

Figure 5. The binding mode between compound **7** and LMW-PTP is unique and can hardly be adopted by the classical PTPs like PTP1B. (A) Sequence alignment and structure superimposition of the signature motif of LMW-PTP and PTP1B (PDBID: 1PXH). The conserved residues are shown and labeled in red; the residue number in PTP1B is shown in parenthesis; the steric conflicts are presented

1
2
3 by solid spheres (atoms in PTP1B) and dotted spheres (atoms in compound 7). These conflicts may exist
4
5 whether PTP1B is in (B) WPD-closed (PDBID: 1PXH) or (C) WPD-open (PDBID: 2HNP)
6
7 conformation.
8
9

10 **Figure 6.** Interaction details for Compound 7 with LMW-PTP. (A) Interaction details represented in 3D
11 space. All residues within 5 Å distance of Compound 7 (carbon in green) are shown in stick (carbon in
12 gray), hydrogen-bonds are shown in yellow dash line. (B) 2D interaction diagram. Hydrogen-bonds are
13 indicated by red dash line with distance labeled. Hydrophobic and π - π interactions are highlighted in
14 green color.
15
16
17
18
19
20
21

22 **Figure 7.** Structure and activity of SPAA inhibitors with various substituents on the α -benzene ring.
23

24 **Figure 8.** Structures of compound 7 derivatives and their inhibitory activities against LMW-PTP.
25
26

27 **Figure 9.** Cellular effect of compound 28 on insulin induced AKT phosphorylation in HepG2 cells. (A),
28 compound 28 dose dependently enhanced AKT phosphorylation. (B), compound 33, a structurally
29 related but inactive analog, had no effect on AKT phosphorylation. The bands were quantified by Image
30 J, and the ratios of pAKT/AKT were normalized to the vehicle control.
31
32
33
34
35
36
37
38
39
40
41
42
43
44
45
46
47
48
49
50
51
52
53
54
55
56
57
58
59
60

Figure 1

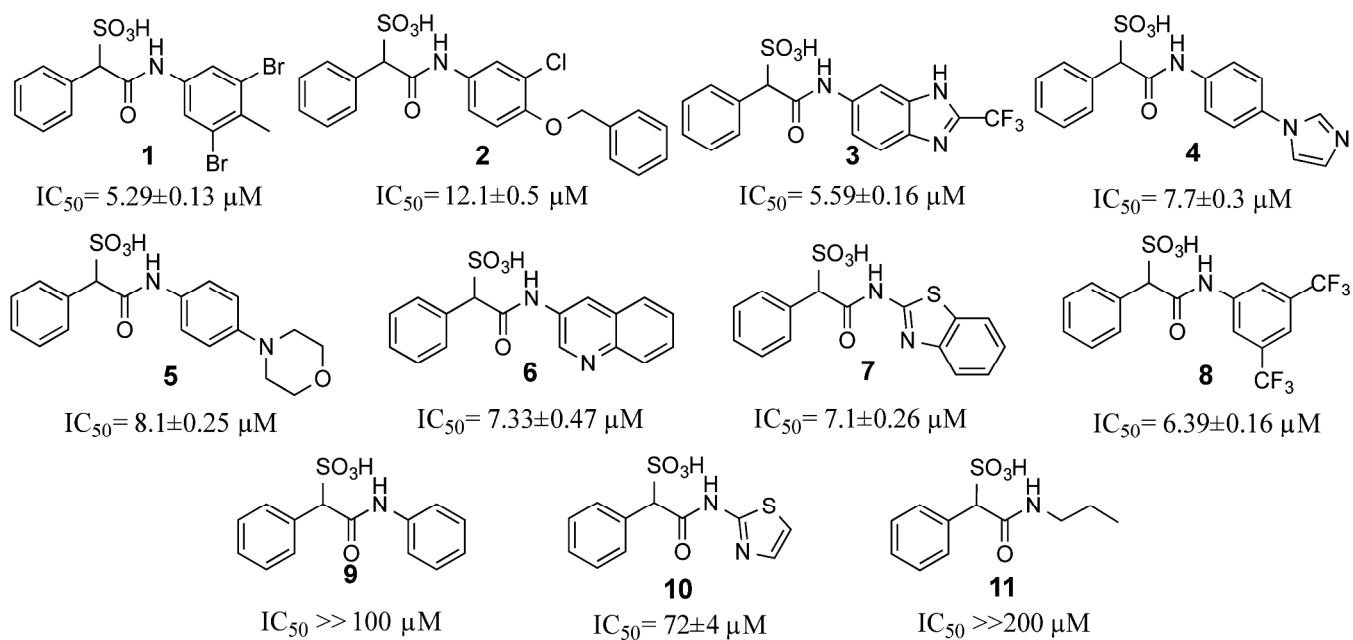


Figure 2

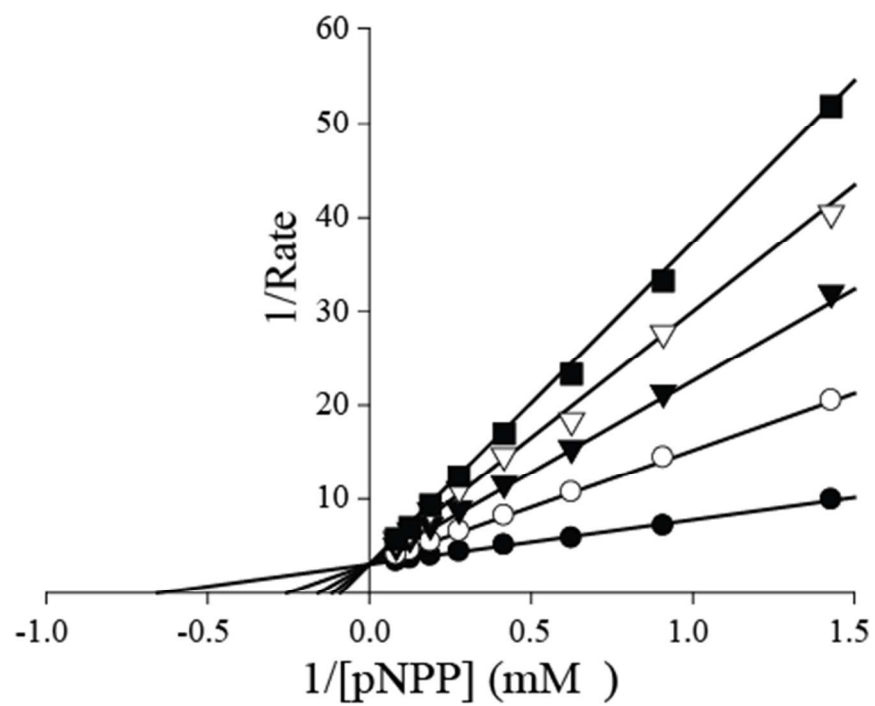


Figure 3

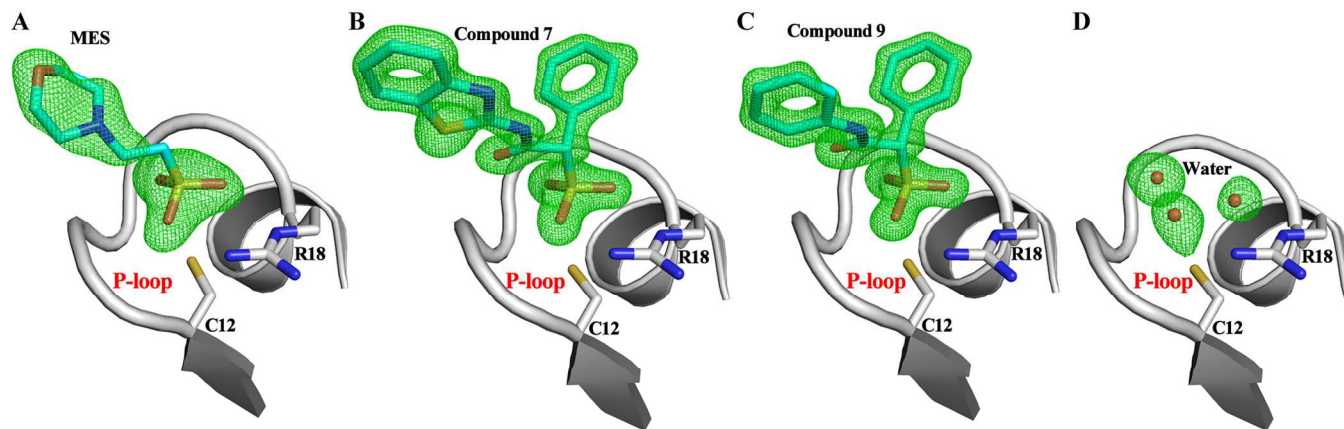


Figure 4

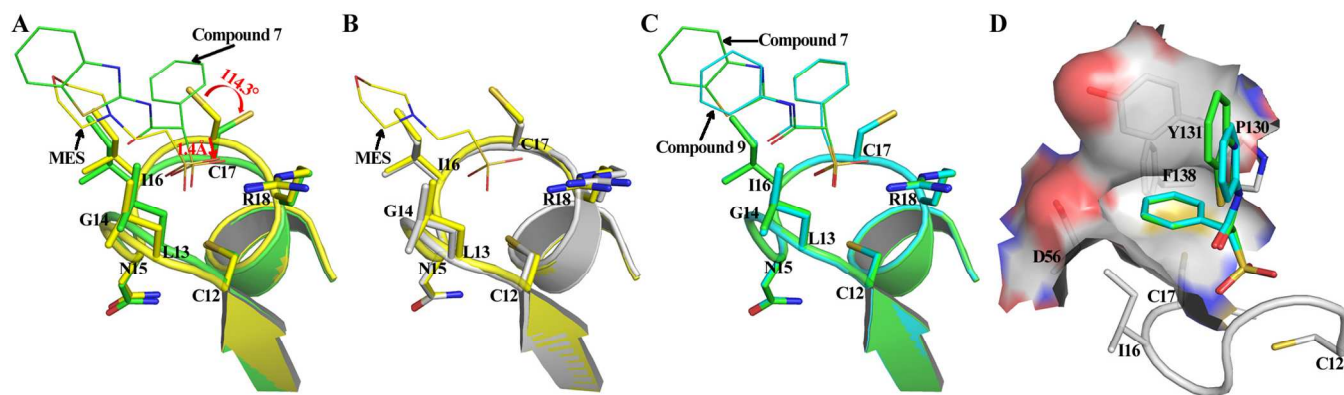


Figure 5

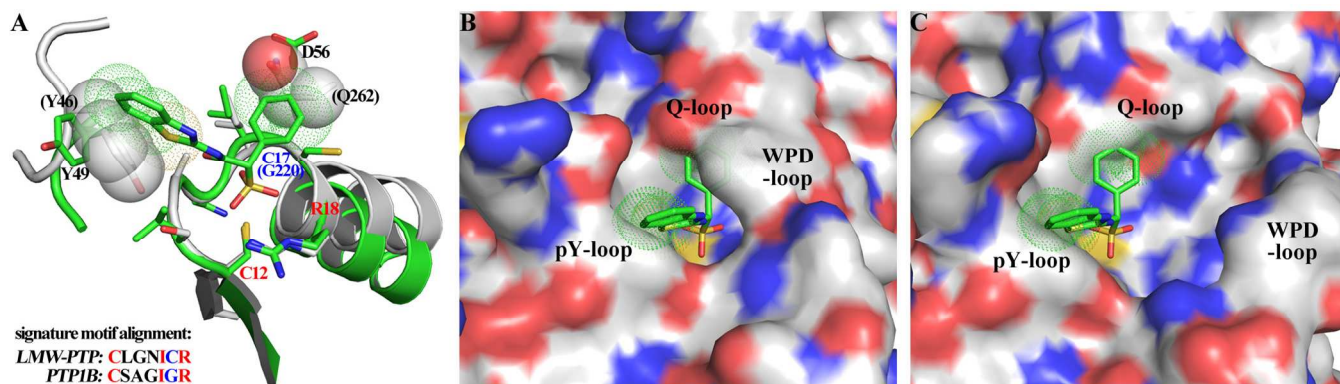


Figure 6

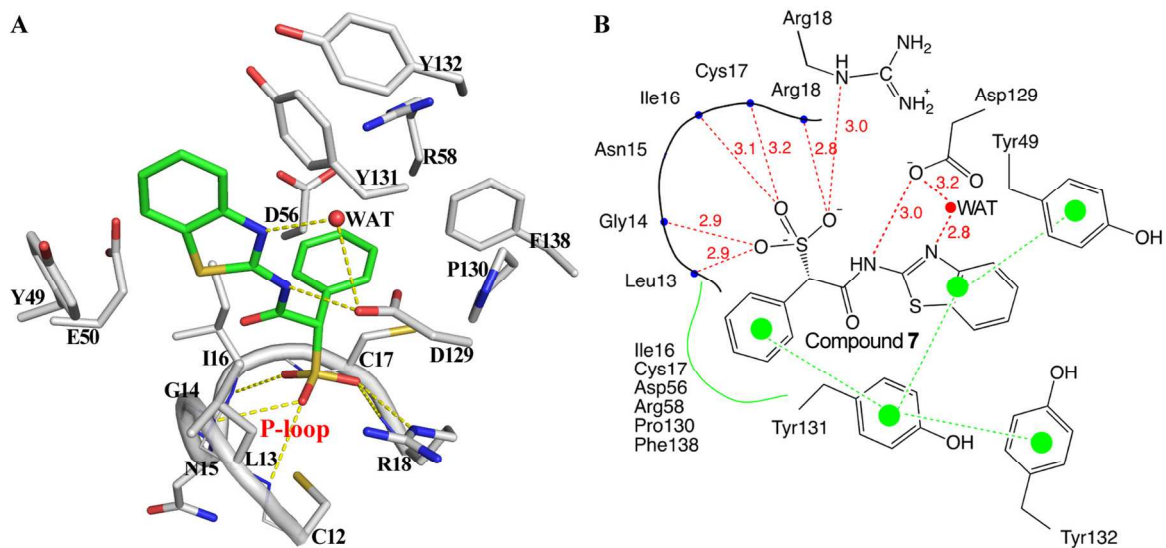


Figure 7

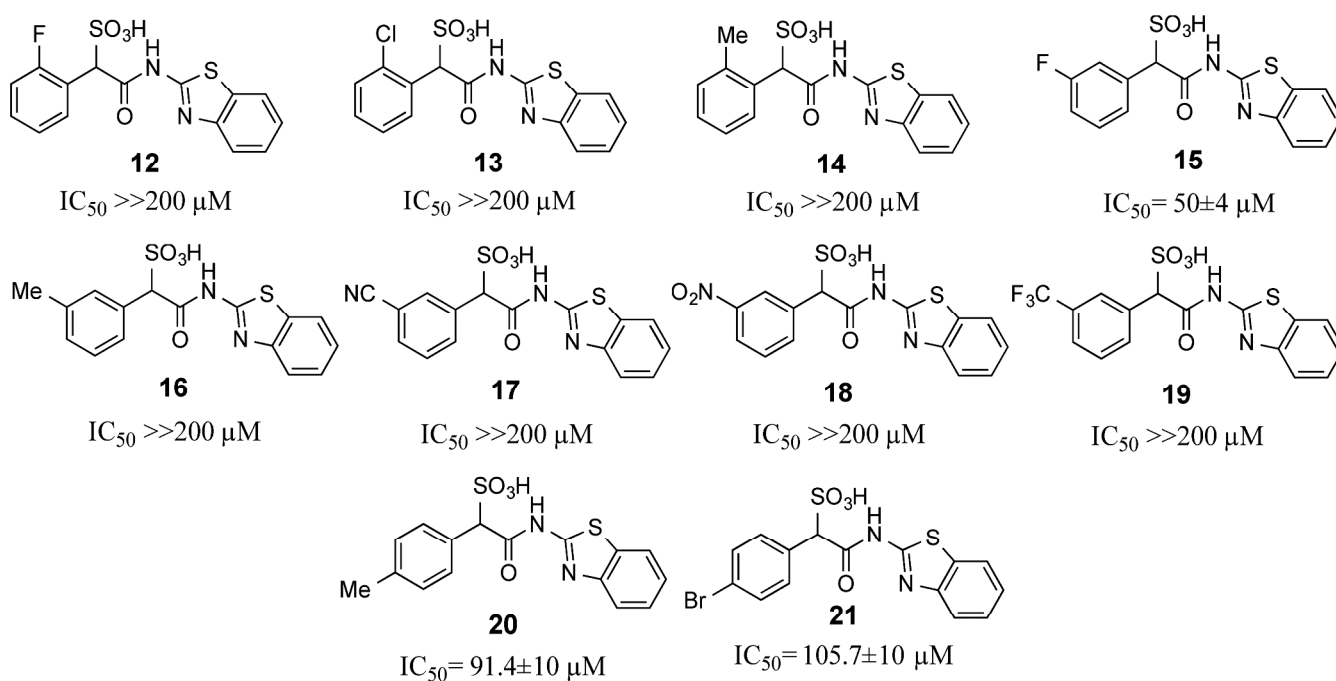


Figure 8

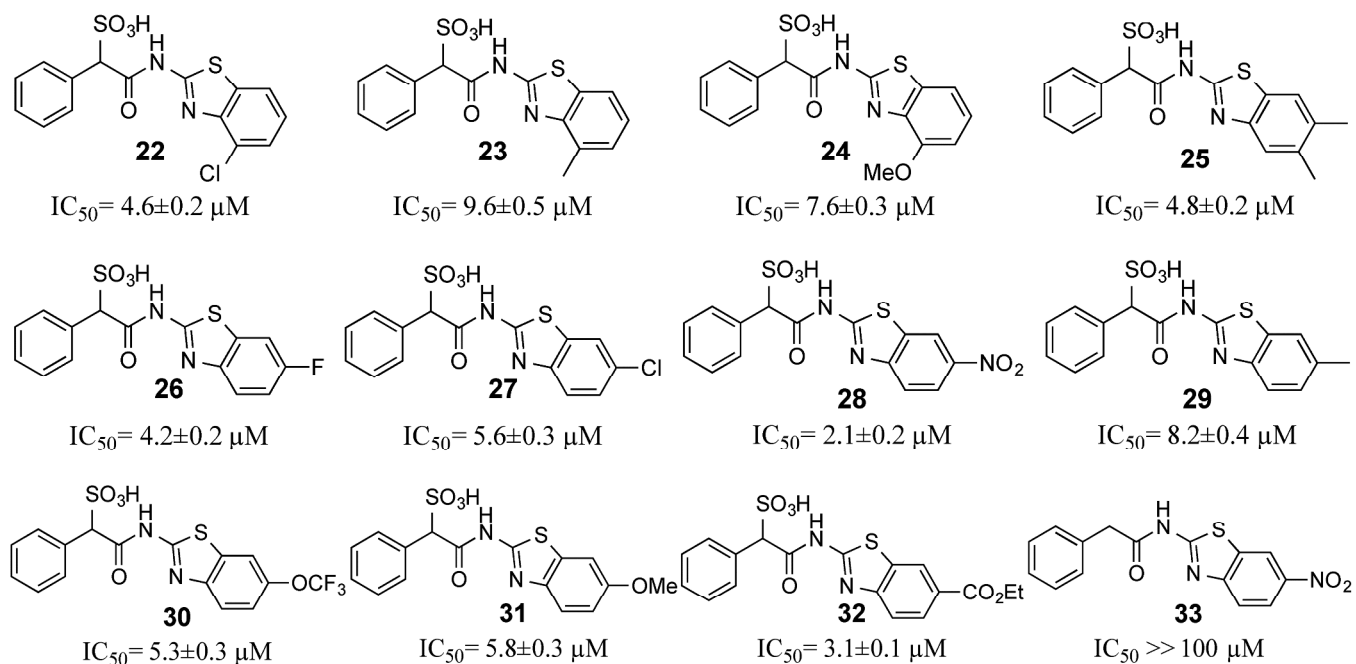


Figure 9

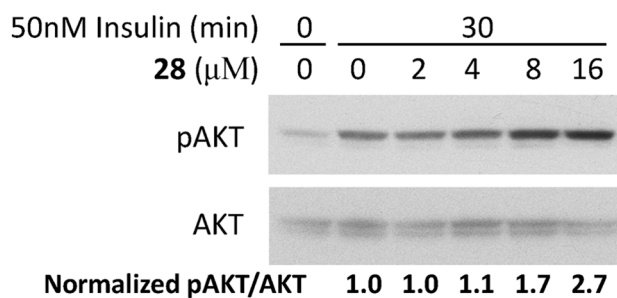
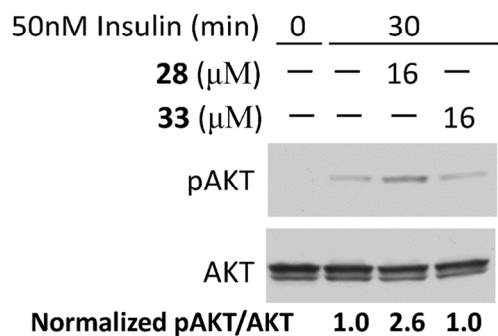
A**B**

Table 1. IC₅₀ of selected compounds against LMW-PTP and 24 other PTPs with pNPP as a substrate.

	1	2	3	4	5	6	7	8	28
LMW-PTP	5.3	12.1	5.6	7.7	8.1	7.3	7.1	6.4	2.1
SHP2	>>200	>>200	>>200	>>100	>>200	>>200	>>200	>>200	>>100
PTP1B	>>200	>>200	>>200	>>100	>>200	>>200	>>200	>>200	>>100
TC-PTP	>>200	>>200	>>200	>>100	>>200	>>200	>>200	>>200	>>100
SHP1	>>200	>>200	>>200	>>100	>>200	>>200	>>200	>>200	>>100
LYP	>>200	>>200	>>200	>>100	>>200	>>200	>>200	>>200	>>100
HePTP	>>200	>>200	>>200	>>100	>>200	>>200	50.0	94.0	>>100
Meg2	>>200	>>200	>>200	>>100	>>200	>>200	>>200	>>200	>>100
PTPH1	>>200	>>200	>>200	>>100	>>200	>>200	>>200	>>200	>>100
FAP-1	>>200	73.5	>>200	>>100	>>200	>>200	34.0	76.0	>>100
PEST	72.3	69.9	>>200	>>100	>>200	>>200	43.5	66.9	>>100
CD45	>>200	>>200	>>200	>>100	>>200	>>200	>>200	>>200	>>100
LAR	>>200	>>200	>>200	>>100	>>200	>>200	>>200	>>200	>>100
PTP α	>>200	>>200	>>200	>>100	>>200	>>200	>>200	>>200	>>100
PTP β	>>200	>>200	>>200	>>100	>>200	>>200	>>200	>>200	>>100
PTP γ	>>200	>>200	>>200	>>100	>>200	>>200	>>200	>>200	>>100
PTP ϵ	>>200	>>200	>>200	>>100	>>200	>>200	>>200	>>200	>>100
PTP σ	>>200	>>200	>>200	>>100	>>200	>>200	>>200	>>200	>>100
PTP μ	>>200	>>200	>>200	>>100	>>200	>>200	>>200	>>200	>>100
MKP3	>>200	>>200	>>200	>>100	>>200	>>200	>>200	>>200	>>100
VHR	>>200	>>200	>>200	>>100	>>200	>>200	>>200	>>200	>>100
VHZ	>>200	>>200	>>200	>>100	>>200	>>200	>>200	>>200	>>100
CDC14A	>>200	>>200	>>200	>>100	>>200	>>200	>>200	>>200	>>100
SSu72	>>200	66.6	>>200	>>100	>>200	>>200	69.9	83.0	>>100
PP5	>>200	>>200	>>200	>>100	>>200	>>200	>>200	>>200	>>100

Table 2. Data collection and structure refinement statistics.

	LMW-PTP•7	LMW-PTP•9	LMW-PTP•MES	LMW-PTP
Data Collection				
Space group	$P2_12_12_1$	$P2_12_12_1$	$P2_12_12_1$	$P2_12_12_1$
Cell dimensions				
<i>a</i> (Å)	34.801	34.190	33.690	31.957
<i>b</i> (Å)	53.963	54.573	54.826	55.453
<i>c</i> (Å)	97.330	97.515	95.191	96.326
$\alpha=\beta=\gamma$ (deg)	90.0	90.0	90.0	90.0
Resolution (Å)	50.00-1.50	50.00-1.45	50.00-1.91	25.00-2.05
Total observations	182980	233460	94514	75930
Unique observations	28910	33262	14276	11281
Completeness (%)	95.5 (74.5)	99.9 (100.0)	99.7 (100.0)	99.9 (99.6)
Redundancy	6.3 (4.5)	7.0 (6.7)	6.6 (6.6)	6.7 (6.4)
R_{merge} (%)	5.9 (60.7)	7.6 (79.9)	15.8 (79.4)	10.2 (80.2)
$\langle I/\delta(I) \rangle$	27.9 (2.0)	24.4 (1.9)	27.7 (2.9)	25.5 (2.6)
Structure Refinement				
Resolution (Å)	27.81-1.50	21.63-1.45	27.46-1.91	24.03-2.05
No. of reflections used	28731	33197	14231	11197
No. of protein atoms	1280	1257	1225	1238
No. of inhibitor atoms	23	32	12	n.a.
No. of water	228	268	121	69
$R_{\text{work}}/R_{\text{free}}$	0.167/0.194	0.164/0.177	0.185/0.228	0.193/0.266
rms deviations				
Bond length (Å)	0.006	0.006	0.008	0.008
Bond angle (deg)	1.175	1.095	1.989	1.066
Average B factors (Å ²)				
Protein	18.43	15.90	32.29	36.02
Water	32.90	29.39	37.93	37.57
Inhibitor	12.49	12.10	30.48	n.a.
All atoms	20.59	18.24	32.79	36.10

The data were collected from a single crystal. Values in parentheses are for highest-resolution shell.

Table of Contents Graphic

